BubR1 and Mad2 regulate adult midgut remodeling in *Drosophila* diapause

Yuya Adachi[1], Hiroki Nagai[1,2], Takako Fujichika[3], Aya Takahashi[3], Masayuki Miura[1], and Yu-ichiro Nakajima[1]*

1. Graduate School of Pharmaceutical Sciences, The University of Tokyo, Japan
2. Institute of Science and Technology Austria, Austria
3. Department of Biological Sciences, Tokyo Metropolitan University, Japan

*Author for correspondence e-mail: nakaji97@g.ecc.u-tokyo.ac.jp

Tel: +81-3-5841-4863

Text: 27,908 characters

Figures: 5

Supporting information: Supplemental figures S1-S4, Supplemental table S1-S5

Summary

Diapause is a survival strategy in which growth and aging are temporarily suspended, enabling animals to withstand unfavorable environments. Various insects, including the fruit fly *Drosophila*, enter reproductive diapause, or dormancy, in response to cold temperatures and/or short-day lengths. During reproductive diapause, ovarian development halts, and non-reproductive organs also undergo remodeling at both morphological and metabolic levels: however, the mechanisms underlying this remodeling and its physiological impact remain largely unclear. Here, we show that the *Drosophila* adult midgut undergoes extensive remodeling in diapause, marked by a sustained growth arrest due to the cell cycle arrest of intestinal stem cells (ISCs), reverting to normal upon returning to recovery conditions. During dormancy, BubR1 and Mad2, key regulators of mitosis, are highly expressed and localized in the cytoplasm of ISCs rather than at the kinetochore, and both BubR1 and Mad2 are essential for diapause-specific midgut remodeling. Furthermore, disruption of midgut growth arrest during diapause reduces the resistance to starvation in adult flies. Therefore, our findings identify a novel role for BubR1 and Mad2 in ISCs, promoting proper midgut remodeling during dormancy, and highlight the importance of this process for survival under adverse environments.

Introduction

Wild animals have developed survival strategies to cope with harsh environmental conditions, such as temperature fluctuations, drought, and food shortages. Among these strategies, dormancy programs—including hibernation, torpor, and diapause—are critical adaptations that involve a reduction in metabolic rate and body temperature, which conserves energy, extends lifespan, and increases the probability of survival for the species (Easwaran & Montell, 2023; Staples, 2016; Wilsterman et al., 2021). By temporarily halting growth and delaying organ development under stressful conditions such as starvation and low temperatures, dormancy helps reduce the energy expenditure required for growth and reproduction, and such synchronization of physiological processes with environmental conditions enhances the organism's ability to survive (Denlinger, 2022; Schiesari & O'Connor, 2013). Understanding the underlying mechanisms of dormancy may thus provide valuable insights into the regulation of stress resistance, aging, and reproduction.

Dormancy programs typically comprise three distinct phases: a preparatory phase, in which environmental cues initiate dormancy; a dormancy phase, characterized by reduced metabolism and activity; and a recovery phase, where normal growth and activity resume(Gray et al., 1991; Harsimran Kaur Gill et al., 2017) . To enter and exit dormancy at the appropriate time, animals must detect environmental conditions and coordinate internal physiological processes. As such, dormancy regulation generally requires central control mechanisms involving the brain and endocrine systems (Helfrich-Förster, 2024; Karp, 2021). While hormonal and neural regulation play pivotal roles in these processes, peripheral organs and tissues must undergo significant remodeling during dormancy and revert during recovery. For instance, during hibernation in certain mammals (*e.g.* thirteen-lined ground squirrels, Syrian hamsters) and diapause in insects, structural changes are observed in respiratory and digestive organs, as well as muscles and adipose tissues (Kim et al., 2006; Kim & Denlinger, 2009; Kurtz et al., 2021). Nevertheless, the mechanisms by which cellular compositions within individual organs and tissues are precisely coordinated to adjust dormancy programs remain largely unknown.

Various animal species enter dormancy at different life stages, and in adult insects, dormancy is often referred to as reproductive diapause, a state that suppresses reproductive organ development, accompanied by reduced locomotor activity, lower metabolism, increased stress resistance, and extended lifespan (Denlinger, 2022; Tatar & Yin, 2001). In species like *Drosophila*, reproductive diapause is triggered by low temperatures and/or short-day conditions (Hara & Yamamoto, 2022; Lirakis et al., 2018; Ojima et al., 2018; Saunders et al., 1989). As with other diapausing insects, reduction of juvenile hormone and insulin signaling are critical for maintaining reproductive diapause in *Drosophila* (Easwaran et al., 2022; Saunders et al., 1990; Schiesari et al., 2016). Recent studies have used *D. melanogaster* to explore genetic basis of the complex biology of dormancy, including identification of circadian neurons regulating endocrine organs, the mechanism of germline maintenance, and sleeping behaviors (Easwaran et al., 2022; Kurogi et al., 2023; Meiselman et al., 2022; Meyerhof et al., 2024; Schiesari et al., 2016). Interestingly, similar to dormancy programs in other animals, somatic non-reproductive organs such as the midgut undergo structural changes during reproductive diapause in *Drosophila* (Kubrak et al., 2014); however, the mechanism by which dormant state regulates organ remodeling and its physiological impacts remain unclear.

The *Drosophila* adult midgut, composed of a monolayered epithelium surrounded by visceral muscles, is a home to resident intestinal stem cells (ISCs) that self-renew and give rise to committed progenitors, enteroblasts (EBs) and enteroendocrine progenitor cells (EEPs); these progenitors differentiate into the absorptive enterocyte (EC) and secretory enteroendocrine cells (EE), respectively (Hung et al., 2020; Miguel-Aliaga et al., 2018; see also Fig. 2A, 2B). To achieve adaptive responses to environmental changes at the organ level, the ISC lineage exhibit characteristic behaviors, allowing tissue homeostasis and plasticity (Nagai et al., 2022; O'Brien et al., 2011). Furthermore, midgut plays a central role in regulating organism-level physiology, influencing appetite, fecundity, immunity, and lifespan (Malita et al., 2022; White et al., 2021; Yoshinari et al., 2024; Zhou et al., 2020). With its relatively simple structure and conserved cell lineages, the *Drosophila* adult midgut serves an ideal system for dissecting

the mechanisms of organ remodeling associated with environmental challenges including dormancy.

Here, we investigate the mechanism of organ remodeling during diapause, using the *Drosophila* adult midgut as a model. Our results show that intestinal growth halts during dormancy and resumes during recovery, accompanied by changes in structural and metabolic gene expression. We identify mitotic regulators BubR1 and Mad2, which are highly expressed in the cytoplasm of ISCs, as key players in midgut remodeling during diapause, and disruption of these genes leads to abnormal gut size and a reduced capacity for starvation resistance. These findings suggest novel roles of BubR1 and Mad2 in controlling ISCs dynamics and contributing to midgut remodeling in *Drosophila* diapause.

Results

The adult midgut of *D. melanogaster* undergoes remodeling in response to diapause and recovery

In adult females of *D. melanogaster*, reproductive diapause can be induced by exposing newly-eclosed flies to cold temperatures (below 12°C), halting ovarian development at an early stage (Anduaga et al., 2018). Following previous studies (Easwaran et al., 2022; Kubrak et al., 2014; Saunders et al., 1989), we kept newly-eclosed flies at short-day photoperiods (10L:14D) and 10°C while non-diapause control flies were kept at 12L:12D and 18°C (Fig. 1A). Under such a suboptimal condition, females entered reproductive dormancy as no yolk accumulation was observed in the ovaries (Fig. S1A). To assess changes in midgut size during diapause, we measured the length and area of the midgut in the wild-type fly (Canton-S) under diapause and non-diapause conditions for 1 to 5 weeks. Consistent with the previous finding (Kubrak et al., 2014), we confirmed that the midgut length remained shorter during diapause compared to non-diapause conditions (Fig. 1B, 1C), while it is similar to that immediately after eclosion (Fig. 1C). After one week of recovery from diapause, the midgut significantly increased in size (Fig. 1B, 1D, Fig. S1B, S1C) and fully recovered by day 4 (Fig. S1D). Of note, after 5 weeks of diapause, no significant midgut growth

occurred upon recovery (Fig. 1D), suggesting the existence of a time limit on the midgut's ability to regrow. These findings together indicate that the midgut halts growth during diapause but remains capable of rapid regrowth upon recovery.

The *Drosophila* adult midgut consists of anterior (R1-R2), middle (R3), and posterior regions (R4-R5) (Buchon et al., 2013; Marianes & Spradling, 2013). Since these regions respond differently to environmental changes due to the different nature of ISCs and their progenies (Li & Jasper, 2016; Mattila et al., 2024; Nagai et al., 2023; O'Brien et al., 2011), we analyzed midgut size changes in anterior and posterior regions under the 3-week diapause condition where the difference of the midgut size between diapause and non-diapause is most significant (Fig. 1C). We found that the posterior midgut exhibited the more significant difference (Fig. 1E), compared to the anterior midgut. Similar region-specific gut resizing during diapause and recovery was also observed in the w^{1118} strain (Fig. 1F), suggesting that the posterior region is preferentially affected during dormancy. It has been reported that reproductive development is also suppressed in *Drosophila* adult males under the same conditions where females enter diapause (Kubrak et al., 2016). We thus measured the midgut size in males under diapause and non-diapause conditions and found no significant differences in midgut size between two conditions (Fig. S1G). These observations suggest that midgut remodeling in diapause is a female-specific characteristic.

To determine whether such midgut remodeling is specific to diapause or a general response to cold-induced stress, we exposed female flies to the cold temperature after the midgut had matured in which no diapause was induced (Ojima et al., 2018). Comparing the midgut size under 3 weeks of cold and diapause conditions, we found that midgut size was larger under cold conditions (Fig. S1E, S1F). Furthermore, midgut growth was not observed when flies were transferred from the cold condition to recovery, unlike the recovery from diapause (Fig. S1F). Altogether, these results suggest that midgut remodeling is a diapause-specific response in adult females, with the midgut halting growth in a regrowth-ready state. In this paper, we referred this midgut remodeling during diapause as dormancy-dependent midgut remodeling (DDMR) in the following.

Midgut remodeling as a common response in *Drosophila* species

While the model organism *D. melanogaster* has recently been used as a genetic model to study different aspects of diapause (Easwaran et al., 2022; Easwaran & Montell, 2024; Meiselman et al., 2022; Ojima et al., 2018), it is still unclear whether these flies naturally enter diapause in the wild (Lirakis et al., 2018). In contrast, some species of the genus *Drosophila* are known to undergo a programmed state of diapause in response to environmental changes, such as short-day lengths, allowing them to survive through winter (Kimura, 1990; LAKOVAARA et al., 1972).

To explore whether DDMR is a general organ-level response during reproductive dormancy, we examined two other *Drosophila* species, *D. bifasciata* and *D. triauraria* (Fig. 1G), among which inhabit in northern regions halt ovarian development in short-day seasons (Watabe, 1979; Yamada & Yamamoto, 2011). We confirmed these species exhibit reproductive diapause under the short-day condition (SD, 10L: 14D), while such diapause was not induced in the long-day condition (LD, 16L: 8D) at the same moderate temperature (15°C) (Fig. 1H, S1H). In SD, the midgut size was significantly smaller compared to LD, and midgut regrowth was observed during recovery (Fig. 1I-1K). Notably, such growth arrest of the midgut was not observed in non-diapause strains of *D. triauraria*, originated from southern regions (Yamada & Yamamoto, 2011) (Fig. S1I, S1J). These results support the notion that DDMR in *D. melanogaster* represent a general organ-level response triggered during diapause in the genus *Drosophila*.

ISCs are in cell cycle arrest and inhibition of mitosis during diapause

In the adult midgut epithelium of *Drosophila*, ISCs serve as resident stem cells, maintaining the self-renewing population and producing progenitors, EBs and EEPs, which further differentiate into absorptive ECs and secretory EEs, respectively (Fig. 2A, 2B; Hung et al., 2020; Miguel-Aliaga et al., 2018). Previous studies have shown that alterations in cell number via ISC expansion and reduction contribute to the significant change in midgut size in response to environmental fluctuations (Christensen et al., 2024; Nagai et al., 2022; Stojanović et al., 2022). For example, after mating, juvenile hormones stimulate ISC proliferation, leading to an increase in midgut size (Reiff et al., 2015). Similarly, upon refeeding following starvation, ISC symmetric division is

214 promoted in the posterior midgut (O'Brien et al., 2011), resulting in ISC
215 expansion followed by an increase in total cell number as well as midgut size.
216 To investigate whether changes in cell number contribute to midgut
217 remodeling in diapause, we first quantified the cell abundance in the midgut
218 following 3 weeks of diapause. We observed a significant reduction in total cell
219 number during diapause compared to non-diapause conditions (Fig. 2C). We
220 then examined the number of ISC/EB lineage using the protein trap line *esg-*
221 *GFP.* The number of *esg*+ cells, along with their proportion, was markedly
222 lower, especially in the posterior midgut during diapause (Fig. 2D, 2E, Fig.
223 S2A). Consistent with this observation, the ISC marker *Delta* (*Dl*) and the EB
224 marker *Su(H)* exhibited reduced expression in the diapausing midgut (Fig. S2B-
225 S2F). Moreover, *esg*+ cell number dramatically increased during recovery from
226 diapause, coinciding with midgut regrowth (Fig. 2E). These findings suggest a
227 possibility that ISCs remain in a non-proliferative state during diapause and
228 resume proliferation upon recovery.
229 To test this possibility, we investigated ISC mitotic activity using the
230 anti-phospho-Histone H3 (PH3) immunostaining, a marker for mitotic cells.
231 Unexpectedly, we found that the number of ISCs in the M phase significantly
232 increased in both the anterior and posterior midgut during diapause (Fig. 2F,
233 2G). Despite the reduced number of ISCs (Fig. 2E, S2B, S2C), the increase in
234 mitotic cells suggests that ISCs may arrest the cell cycle in the M phase or
235 experience prolonged M phase during diapause. In order to directly test ISC
236 proliferative capacity, we conducted clonal expansion assays using the mosaic
237 analysis with a repressible cell marker (MARCM) system (Fig. 2H) and found
238 that clonal size was significantly reduced during diapause, with fewer ISCs
239 present in the clones (Fig. 2I, 2J). This mitotic arrest was not observed during
240 recovery from diapause, with the number of mitotic cells returning to non-
241 diapause levels (Fig. S2G). To further examine the cell cycle state in ISC
242 lineage, we employed the Fly-FUCCI system (Zielke et al., 2014) in combination
243 with the *esg-QF* driver during diapause. Using this system that allows
244 monitoring of cell cycle at cold temperatures, we found that a significantly higher
245 proportion of *esg*+ cells were in the G2/M phase during diapause compared to
246 non-diapause controls (Fig. 2K, 2L). Additionally, using the *CycB-GFP* line, we

247 confirmed increased *CycB* expression in ISCs during diapause (Fig. S2H),
248 reinforcing the idea that ISCs arrest in the G2/M phase. These results suggest
249 that ISCs undergo cell cycle arrest in the G2/M phase during dormancy.
250 Combined, our findings reveal that ISCs undergo drastic behavioral
251 changes during DDMR where ISCs halt the cell cycle at a recoverable state,
252 reducing the number of cells produced post-eclosion and allowing for proper
253 size change during diapause.
254
255 **Molecular signatures of DDMR**
256 To explore the molecular signature of DDMR, we conducted a transcriptome
257 analysis of the midgut. Specifically, bulk RNA sequencing (RNA-seq) was
258 performed using samples of the entire adult midgut from two conditions: 3 weeks
259 diapause (3wD), 3 weeks non-diapause control (3wC). We identified 3,391 genes
260 that were differentially expressed during dormancy (Fig. 3A). Gene Ontology
261 (GO) enrichment analysis and Reactome pathway analyses revealed metabolic
262 processes, including small molecule, lipid, and carboxylic acid metabolism were
263 significantly enriched in the 3wD midgut (Fig. S3A, S3B), suggesting that large-
264 scale metabolic remodeling occurs alongside structural changes in the midgut
265 during dormancy. Lipid metabolism-related genes such as *bmm* and *pepck*, along
266 with carbohydrate metabolism-related genes like *tobi*, were differently expressed
267 (Fig. S3C). Additionally, pathways related to metabolism (e.g., Metabolism of
268 lipids), translation regulation (e.g., Translation), and circadian gene degradation
269 (e.g., Degradation of TIM) were among the top processes identified (Fig. S3B).
270 Notably, circadian genes *per* and *tim*, which are upregulated in the whole body
271 during diapause (Kučerová et al., 2016), also showed significantly increased
272 expression in the midgut during dormancy (Fig. S3D). Furthermore, the
273 expression of the antimicrobial peptide *Drs*, downstream of the Toll pathway,
274 dramatically increased during dormancy (Fig. S3E), reflecting enhanced innate
275 immunity, a hallmark of diapause at the organismal level (Kubrak et al., 2014).
276 Among the differentially expressed genes, a detailed enrichment
277 analysis was performed by categorizing the genes into two groups: those
278 upregulated during dormancy and those downregulated. In the upregulated gene
279 group, GO terms associated with cell adhesion (e.g., cell adhesion) and RNA

processing (e.g., regulation of RNA splicing) were identified as top-ranked categories (Fig. 3B). Genes associated with RNA processing and RNA metabolism are also upregulated in the ovaries during diapause, suggesting the existence of dormancy-specific translational regulation conserved across organs (DiVito Evans et al., 2023). In contrast, in the downregulated gene group, GO terms related to metabolic processes (e.g., cellular lipid metabolic process) were prominently enriched (Fig 3C). During diapause, extensive changes in the expression of genes involved in metabolic pathways have been observed throughout the body (Kubrak et al., 2014; Kučerová et al., 2016). These findings suggest that gene expression changes linked to DDMR globally follow a pattern similar to that observed in the entire organism and other organs.

Next, to explore the molecular signature of recovery from DDMR, RNA-seq was performed using samples of the entire adult midgut from two conditions: 3 weeks diapause followed by recovery (3wD+R), and 3 weeks control followed by recovery (3wC+R). We identified 526 genes with significant expression changes between the 3wD+R and 3wC+R midguts (Fig. S3G). GO enrichment and Reactome pathway analyses identified significantly enriched genes associated with muscle differentiation and smooth muscle contraction (Fig. S3H, S3I). Given the extensive structural remodeling of muscles during insect dormancy (Kim et al., 2006; Kim & Denlinger, 2009), these gene expression changes related to muscle structure during recovery may contribute to the resizing of the midgut. Consistent with this finding, *dilp3*, which codes the product secreted by muscles during feeding and promote ISC proliferation (O'Brien et al., 2011), was significantly upregulated in the 3wD+R midgut (Fig. S3J), suggesting growth-promoting interactions between muscle and ISCs during recovery. In addition, neuropeptide genes such as *NPF, Dh31,* and *CCHa2* showed significant increases in expression (Fig. S3J), indicating that hormone secretion from EEs may change during recovery, potentially influencing gut growth and inter-organ communications. Overall, our findings suggest that the midgut undergoes large-scale structural and metabolic remodeling associated with extensive gene expression changes.

BubR1 expression increases in the cytoplasm of ISCs during diapause

313 Since ISC cell cycle are arrested during diapause (Fig. 2), we focused
314 differentially expressed genes categorized under the GO term “cell cycle
315 checkpoint signaling” (Fig. 3D). G2/M phase checkpoint regulators such as
316 *mre11*, *mei-41* showed significant changes, while *CG15237* and *BubR1* were
317 differentially expressed as M-phase checkpoint regulators. These gene
318 expression changes align with ISC behaviors during dormancy such as
319 prolonged mitotic phases and an increased number of the G2/M phase cells.
320 Among such genes, *BubR1* is particularly noteworthy due to its classical role as
321 a mitotic checkpoint regulator and timer during mitosis (Karess et al., 2013), and
322 its expression in ISCs (Shinoda et al., 2023). Importantly, *BubR1* expression
323 increased nearly threefold during diapause (Fig. 3E), suggesting its potential
324 impact on ISC behaviors and midgut remodeling.
325 To investigate *BubR1* expression at the cellular level, we used fly lines,
326 which allow detection of endogenous expression pattern of *BubR1*
327 (*EGFP::BubR1*^{WT} and *GFP-BubR1*) to visualize its expression in midgut cells.
328 During reproductive dormancy, *BubR1* was strongly expressed in the cytoplasm
329 of ISCs, primarily in R4 regions (Fig. 3F, 3G, S3F). Such cytoplasmic
330 localization during diapause contrasts with the localization of BubR1 associated
331 with typical spindle checkpoint during mitosis, where it accumulates around
332 kinetochores (Resende et al., 2018). Indeed, colchicine treatment, which
333 induces mitotic arrest through the spindle assembly checkpoint (SAC), caused
334 strong BubR1 localization around kinetochores in ISCs under non-diapause
335 conditions (Fig. 3H, 3I). In contrast, during diapause, despite ISCs being
336 arrested in mitosis, BubR1 remained cytoplasmic, with minimal signal around
337 the kinetochores (Fig. 3H, 3I). These findings suggest that the role of BubR1
338 during DDMR is likely spindle checkpoint-independent and a unique function in
339 the midgut during the dormancy state.
340
341 **BubR1 expression in ISCs is essential for DDMR**
342 To explore the function of BubR1 in reproductive dormancy, we examined its
343 effects on midgut remodeling using two *BubR1* mutant alleles *BubR1*^{k06109} and
344 *BubR1*^{k03113}. qPCR analysis revealed that midgut *BubR1* expression in
345 diapause-inducing condition was significantly reduced in both heterozygous

346 mutants, with *BubR1*^{k03113} showing 48%, *BubR1*^{k06109} showing 57% expression
347 compared to controls (Fig. 4A). We then measured midgut size during diapause
348 in these mutants and found a significant increase in midgut size compared to
349 control flies (Fig. 4B, 4C). This midgut enlargement was accompanied by an
350 increase in the total cell number and the number of mitotic ISCs as well as the
351 number of *esg*+ cells (Fig. 4D-4F). Importantly, when BubR1 function was
352 rescued in the *BubR1* trans-heterozygous mutant (*BubR1*^{k06109}/*BubR1*^{k03113})
353 with an *EGFP::BubR1*^{WT} transgene (Shinoda et al., 2023), total cell number in
354 the posterior region and mitotic cell number in the midgut returned to levels
355 comparable to controls (Fig. 4C-4E). These results strongly suggest that BubR1
356 is required for proper midgut remodeling during diapause. Notably, no ovarian
357 development was observed in any of the mutants under dormancy conditions,
358 confirming successful induction of ovarian dormancy despite impaired midgut
359 remodeling (data not shown). Furthermore, under non-dormant conditions, no
360 significant differences in midgut size were detected between these mutant
361 backgrounds (Fig. S4A), consistent with the result that the number of mitotic
362 cells did not increase—or even decreased— in *BubR1* mutants (Fig. S4B).
363 Collectively, these results highlight a critical role for BubR1 in DDMR.
364 The results obtained from the mutants could potentially reflect non-
365 autonomous effects of *BubR1* expressed in other tissues. We thus investigated
366 whether DDMR is influenced by BubR1 activity specifically in adult ISCs. To this
367 end, we employed somatic tissue-specific CRISPR-mediated depletion (Bier et
368 al., 2018; Meltzer et al., 2019), combined with the temperature-sensitive Gal80^{ts}
369 system (McGuire et al., 2003) to induce *BubR1* mutations in ISC lineages
370 before eclosion (Fig. 4G, S4C). When adult flies were shifted to dormancy
371 conditions, we observed a significant increase in midgut size in ISC/EB-specific
372 *BubR1* knockout flies (Fig. 4H). Furthermore, the number of total and mitotic
373 cells also increased in these somatic *BubR1* knockout lines (Fig. 4I, 4J).
374 Altogether, our results demonstrate that *BubR1* function in ISCs is essential for
375 midgut remodeling during reproductive diapause.
376 Intriguingly, in *D. bifasciata* and *D. triauraria,* which undergo
377 programmed state of diapause in response to short-day length, *BubR1*
378 expression in the midgut is higher in diapausing flies under SD, compared to

379 non-diapausing flies under LD (Fig. S4D, S4E). These results suggest a
380 potential implication of BubR1 in DDMR for the genus *Drosophila*.
381
382 **The MCC component Mad2 is involved in DDMR**
383 During mitosis, BubR1 forms a complex with Mad2, Bub3, and Cdc20, key
384 components of the mitotic checkpoint complex (MCC), and they function
385 cooperatively at the kinetochores (Musacchio, 2015). From our RNA-seq
386 analysis, we found that, in addition to *BubR1,* the expression levels of *mad2*
387 significantly increased during dormancy (Fig. 5A) while not identified as a
388 differentially expressed gene. Intriguingly, among the MCC, Mad2 can interact
389 with BubR1 in the cytoplasm of mammalian cells to regulate insulin signaling
390 and metabolism (Choi et al., 2016). This raises a possibility that Mad2 may play
391 a critical role in DDMR, independently of its role in the MCC.
392 To test this, we utilized the *GFP-Mad2* line to examine its expression in
393 the adult midgut and found that *mad2* was highly expressed in the cytoplasm of
394 ISCs during diapause (Fig. 5B, 5C), reminiscent of the cytosolic localization of
395 BubR1 (Fig. 3F, S3F). To further investigate the function of Mad2 during DDMR,
396 we analyzed midgut size using two *mad2* mutant alleles, $mad2^{\Delta}$ and
397 $mad2^{EY21687}$. Our analysis revealed that heterozygous *mad2* mutants had
398 significantly larger midguts during dormancy compared to controls (Fig. 5D, 5E).
399 We also found that the number of *esg*+ cells increased in the anterior and
400 posterior region of the midgut (Fig. 5F). These findings suggest that, during
401 reproductive diapause, Mad2 is localized in the cytoplasm of ISCs, similar to
402 BubR1, and that both proteins together regulate DDMR.
403
404 **DDMR enhances starvation resistance**
405 Halting organ growth during dormancy is thought to conserve energy, thereby
406 enhancing survival during periods of scarce food availability, such as winter
407 (Denlinger, 2022). In *Drosophila*, maintaining midgut size during reproductive
408 diapause may contribute to increased resistance to starvation. To test this
409 hypothesis, we compared starvation resistance between *BubR1* mutants with
410 controls in the dormant condition. Although dormancy generally enhances
411 starvation resistance compared to non-dormant states, $BubR1^{k03113}$ mutant flies

412 significantly reduced starvation resistance during dormancy (Fig. 5G). These
413 results suggest that BubR1/Mad2-mediated DDMR plays a critical role in
414 enhancing starvation resistance at the organismal level.
415
416
417 **Discussion**
418 In this study, we demonstrate that BubR1 and Mad2 play crucial roles in DDMR
419 in *Drosophila* by modulating ISC dynamics to achieve diapause-specific states.
420 While BubR1 and Mad2 are well-known as components of the MCC that localizes
421 to the kinetochore, we found that in the diapausing midgut, their localization is
422 predominantly in the cytoplasm of ISCs. Depletion of these proteins causes mis-
423 regulated midgut growth, leading to a reduction in starvation resistance during
424 diapause. Based on these findings, we propose that BubR1 and Mad2 act as key
425 regulators of the ISC cell cycle during diapause, enabling a reversible state that
426 supports recovery (Fig. 5H).
427 The *Drosophila* midgut undergoes extensive remodeling in response to
428 various internal and external stimuli, which directly or indirectly influence ISC
429 activity (Christensen et al., 2024; Nagai et al., 2022; Stojanović et al., 2022).
430 During starvation, for instance, the midgut size decreases as ECs undergo
431 apoptosis, while upon refeeding, ISCs are stimulated by Dilp3 secreted from
432 visceral muscles, promoting symmetrical ISC division and restoring midgut size
433 (O'Brien et al., 2011). Similarly, during reproductive diapause—a condition
434 where food intake is reduced by less than half (Kubrak et al., 2014)—mild
435 starvation responses may also contribute to midgut size reduction. Indeed,
436 reproductive arrest can be more readily induced by adding starvation conditions
437 (Ojima et al., 2018). During recovery, our RNA-seq data revealed increased
438 *dilp3* expression and decreased expression of the FoxO target gene *Thor* (Fig.
439 S3J), suggesting a possibility that Dilp3 secreted from muscles contributes to
440 ISC activation like post-starvation refeeding. However, in contrast to a simple
441 starvation response, midgut cell death is minimal during diapause (Fig.S2I), and
442 ISC cell cycles are arrested at the G2/M in a recoverable state (Fig. 2).
443 Furthermore, during reproductive arrest, germline stem cells in ovaries exhibit
444 behaviors markedly different from those observed during amino acid deficiency

445 responses (Easwaran et al., 2022). Collectively, these findings suggest that
446 organ-level responses during diapause are driven by a complex interplay of
447 environmental factors rather than by a simple starvation-induced mechanism.
448 Across species, developmental diapause often involves a temporary
449 halt in the cell cycle, delaying organ growth. For example, during pupal
450 diapause in the flesh fly brain and embryonic diapause in the turquoise killifish,
451 the cell cycle primarily arrests at the G0/G1 phase (Meller et al., 2012;
452 Tammariello & Denlinger, 1998). In contrast, most cells in silkworm embryos are
453 arrested in the G2 phase during diapause (Nakagaki et al., 1991). In this study,
454 we observed a significant increase in ISCs arrested at the G2/M phase during
455 DDMR. Since *Drosophila* oogenesis arrests during diapause due to activation of
456 the Chk2 DNA damage checkpoint (Easwaran et al., 2022), our findings
457 suggest that similar mechanisms may govern growth arrest in the midgut.
458 Indeed, genes such as *mre11* which are differentially expressed in the
459 diapausing midgut (Fig. 3D) are required for G2/M checkpoint activation (Song,
460 2005). Notably, ISCs exhibit active cell cycle arrest during diapause via
461 checkpoint mechanisms, rather than undergoing a passive delay induced by
462 low temperatures (Fig. S1E-S1F). Such controlled cell cycle arrest in resident
463 stem cells may contribute to halting organ growth in other diapausing or
464 hibernating animals and to facilitating rapid recovery once stem cell division
465 resumes.
466 BubR1 is a highly conserved eukaryotic protein that functions as a key
467 component of the SAC, forming the MCC with Mad2, Bub3, and Cdc20 to
468 prevent premature progression of cell division and ensure accurate
469 chromosomal segregation; its disruption increases the risk of aneuploidy (Baker
470 et al., 2013; Karess et al., 2013; Resende et al., 2018). Beyond these canonical
471 functions, studies across cellular to organismal contexts have uncovered
472 additional roles for BubR1. For example, in mouse embryonic fibroblasts,
473 *BubR1* heterozygosity reduces *p53* and *p21* expression after DNA damage,
474 impairing proper G2/M phase arrest (Fang et al., 2006). Additionally, BubR1,
475 together with Mad2, recruits adaptor protein 2 to the insulin receptor (IR) to
476 promote IR endocytosis and reduce insulin sensitivity (Choi et al., 2016; Park et
477 al., 2023; Tang et al., 2020). Consistent with these roles, *BubR1* deficiency in

mice leads to premature aging and reduced lifespan, highlighting its role in organism-wide responses (Baker et al., 2004). In *Drosophila*, BubR1 in the fat body negatively regulates *bmm* expression via IMD signaling during starvation, suppressing lipid breakdown and enhancing lifespan (Liu et al., 2024). These findings underscore a complex regulatory network involving BubR1 and associated proteins across different biological contexts. Although the regulation and interacting partners of BubR1 and Mad2 during diapause remain unclear, the observed changes in their expression in ISCs likely contribute to organism-level responses, including enhanced starvation resistance mediated by structural and metabolic changes in the midgut. Future investigations into the non-canonical role of BubR1 and Mad2 will lead to a better understanding of organ remodeling in dormant programs and provide new insights into the control of resident stem cells.

Acknowledgements

We thank R. Giet, B. Ohlstein, C. Sunkel, N. Shinoda, BDSC, Kyoto Stock Center, NIG-FLY, KYORIN-Fly, and Developmental Studies Hybridoma Bank (DSHB) for fly stocks and reagents; Y. Hara and S. Kondo for discussion.

Funding

This work was supported by JSPS/MEXT KAKENHI (grant numbers JP22J01430 to H.N., JP21H04774, JP23H04766, JP24H00567 to M.M., and JP17H06332, JP22H02762, JP23K18134, JP23H04696 to Y.N.), AMED-PRIME (JP22gm6110025 to Y.N.), The Mochida Memorial Foundation for Medical and Pharmaceutical Research (Y.N.), The Cell Science Research Foundation (Y.N.), and Sadako O. Hirai Ban Award for Young Researchers (H.N.)

Author contributions

Conceptualization: Y.A., Y.N.

Investigation: Y.A., H.N., Y.N.

Methodology: Y.A., H.N., T. F., A.T., Y.N.
Validation: Y.A., H.N., M.M., T. F., A.T., Y.N.
Data curation: Y.A., Y.N.
Writing – original draft: Y.A., H.N., Y.N.
Writing – review & editing: Y.A., H.N., M.M., Y.N.
Supervision: M.M., Y.N.
Funding acquisition: H.N., M.M., Y.N.

Declaration of interests

The authors declare no competing interests.

Materials and methods

Drosophila stock and maintenance

All stocks were maintained on a standard diet containing 4% cornmeal, 6% baker's yeast (Saf Yeast), 6% glucose (Wako, 049-31177), and 0.8% agar (Kishida chemical, 260-01705) with 0.3% propionic acid (Tokyo Chemical Industry, P0500) and 0.05% nipagin (Wako, 132-02635).

Canton-S was utilized as the wild-type strain. Transgenic fly lines were obtained from the Bloomington Drosophila Stock Center (BDSC), NIG-Fly and the Kyoto Stock Center. Unless otherwise indicated, strain descriptions can be found at Flybase (http://flybase.bio.indiana.edu): *Dl-lacZ* (Röttgen et al., 1998) (BDSC 11651), *esg-QF2* (Nagai et al., 2023), *QUAS-Fly-FUCCI* (Zielke et al., 2014) (BDSC 55108), *BubR1*^{k03113} (Kyoto 102258), *BubR1*^{k06109} (Kyoto 102444), *mad2*^{EY} (Bellen et al., 2011) (BDSC 22495), *tub-Gal80*^{ts} (BDSC 7017, 7019, described in Flybase and BDSC), *esg-Gal4* (Goto & Hayashi, 1999) (Kyoto 109126), *UAS-GFP* (BDSC 1521), *UAS-Cas9.T2A.eGFP* (Trivedi et al., 2020) (BDSC 94298), *FRT40A* (originated from BDSC 5074), *attP40{U6-gRNA}* (NIG 2RG-1578). Following lines are gifts from fly community: *esg-GFP[P01986]* (Le Bras & Van Doren, 2006), *Su(H)GBE-lacZ* (Furriols & Bray, 2001), *yw hs-flp; tub-Gal80 FRT40A; tub-Gal4 UAS-dsRed /TM6B* (Guo et al.,

541 2013), *EGFP::BubR1*^{WT} (Shinoda et al., 2023), *GFP-BubR1, GFP-Mad2* (Buffin
542 et al., 2005), *mad2*$^{\Delta}$ (Buffin et al., 2007), *CycB-GFP* (Huang & Raff, 1999).
543 Following other *Drosophila* species were obtained from KYORIN-Fly: *D.*
544 *bifasciata* (JZK3), *D. triauraria* (TM15-92), *D. triauraria* (KMJ1), *D. triauraria*
545 (OEB12). See Additional file: Table S1 for genotypes in each figure. We used
546 female flies unless otherwise noted in the figures.
547
548 **Diapause and recovery induction**
549 To assess the effects of diapause on midgut growth using *D. melanogaster*, we
550 subjected less than 6 h old virgin females to 10°C and 8 L:16D photoperiods
551 (Diapause condition), 18°C at 12L:12D photoperiod (Control condition) for 1-5
552 week. We then allowed the flies to recover by transferring them into vials with
553 fresh food with dry yeast for 7 days at 25°C and 12L:12D photoperiod (Recovery
554 condition).
555 To assess the effects of cold condition on midgut size, we allowed the
556 flies to grow in 18°C for 4 days after eclosion, and then subjected them to 10°C
557 and 8 L:16D photoperiods for 3 weeks (Cold condition).
558 To assess the effects of diapause state on midgut growth in other
559 *Drosophila* species, we subjected less than 6 h old virgin females to 10 L:14D
560 photoperiods (SD, diapause), 16L:8D photoperiod (LD, control) for 16 days.
561 Rearing temperature was always fixed at 15°C. We then allowed the flies to
562 recover by transferring them into 16L:8D photoperiod condition.
563
564 **MARCM clone induction scheme**
565 For the mosaic analysis with a repressible cell marker (MARCM) analysis,
566 MARCM-ready flies (*hsFLP; tub-Gal80,FRT40A/FRT40A; tub-Gal4,UAS-dsRed*)
567 were cultured at 25°C during all of pupal development (except during heat shock
568 induction). When female larvae began metamorphosis, white pupae were placed
569 into an empty vial at 25°C and designated as being at 0 h after puparium
570 formation (APF). MARCM labels one of the two daughter cells after mitotic
571 division. To label dividing ISCs, MARCM-ready flies were heat shocked at 48 h
572 APF for 1 h (time when ISCs are undergoing asymmetric divisions (Guo &
573 Ohlstein, 2015)). After eclosion, the size of the growing ISC clones was observed

with anti-Pros immunofluorescence staining under 1 week diapause or 1 week control conditions. EE-only clones, which can be induced by labeling daughter EE during asymmetric division were excluded by immunostaining against the EE marker Pros, and the size of clones containing two or more ISCs was quantified.

Tissue-specific somatic mutation of BubR1

Transgenic flies expressing BubR1-sgRNA (GGTGACGCCAGTTACTATTG) obtained from NIG gRNA stock collections were crossed to flies expressing *esg*^{ts}*>Cas9* (*esg-Gal4 tubGal80*^{ts} */ CyO; UAS-Cas9 / TM3, Act-GFP*). Experimental crosses were maintained at 18°C to utilize Gal80^{ts} for suppressing Gal4 activity. When female larvae began metamorphosis, white pupae were placed into an empty vial at 18°C. After 6 days, the time when ISC division was completed, pupae were transferred to 29°C and reared for 1 day to introduce somatic mutations. These pupae were then transferred back to 18°C, reared under diapause or control conditions for 3 weeks after eclosion.

Immunofluorescence

Adult midgut samples were dissected in 1 × PBS and fixed in 4% PFA for 30–45 min at room temperature (RT). The following primary antibodies were used with indicated dilution into 1 × PBS containing 0.5% BSA and 0.1% Triton X-100: rabbit anti-PH3 (Millipore 06–570, 1:1000), mouse anti-Prospero (DSHB MR1A, 1:100), rat anti-GFP (Nacalai tesque 04404–26, 1:400), rabbit anti-cDcp1 (Cell Signaling Technology 9578, 1:200), chicken anti-β-galactosidase (Abcam ab9361, 1:500), mouse anti-Delta (DSHB C594.9B, 1:100). After overnight incubation with primary antibodies at 4°C, samples were incubated with fluorescent secondary antibodies (Jackson ImmunoResearch and Invitrogen, 1:500) for 1 h at RT. Hoechst 33,342 (Invitrogen, final concentration: 10 μg/ml) was used to visualize DNA. Samples were mounted in Slowfade Diamond (ThermoFisher, S36963) and imaged with the confocal microscope Zeiss LSM880.

RT-qPCR

Total RNA was purified from 7-10 midguts using the ReliaPrep RNA Tissue Miniprep System (Promega). cDNA was made from 100 or 200 ng of RNA using

PrimeScript RT Reagent Kit (TaKaRa). Quantitative PCR was performed using TB Green Premix Ex Taq II (TaKaRa) and the QuantStudio 6 Flex Real-Time PCR System (ThermoFisher). *RpL32* was used as an internal control. Primers for *D. bifasciata* and *D. triauraria* were designed based on the sequence homology to *D. melanogaster* transcripts. Primer sequences are listed in Additional file: Table S2.

Bulk RNA-seq

Total RNA was purified from 10 to 15 midguts using the ReliaPrep RNA Tissue Miniprep System (Promega). The NanoDrop (ThermoFisher) was used to measure the concentration of each RNA sample, and the integrity of RNA samples was checked using Bioanalyzer. Total 300 ng RNA for each sample was used for cDNA library preparation and the subsequent sequencing was performed on an DNB sequencing system with single reads of 50 base pairs. The sequencing reads were aligned against the *Drosophila melanogaster* genome (ENSEMBL, BDGP6.22) using Salmon (Patro et al., 2017) for transcript quantification. The quantification data of each transcript was converted into gene-level counts using Tximport (Soneson et al., 2015). Differential expression analysis of two conditions/groups (four biological replicates per condition) was performed using the DESeq2 R package (ver 3.20). Genes with an adjusted *P*-value < 0.1 were assigned as differentially expressed. For functional cluster analysis of DEGs, GO BP enrichment analysis and Reactome pathway analysis were performed by the ClusterProfiler R package.

Colchicine treatment

0.2 mM Colchicine were dissolved in 5% (w/v) sucrose solution. Filter paper (Whatman 3MM) was soaked with 300 μL of reagents and placed into empty vials. Newly-eclosed flies were transferred into these vials and fed with 5% sucrose only (control) or colchicine solutions for 1 day.

Starvation resistance

To assay the starvation resistance, flies were fed with agar only food. For the survival assay, dead flies (determined by immobility and showing no response to

640 tapping) were counted every day.
641
642 **Quantification of midgut size**
643 The central line length and area of the midgut were quantified using the
644 Fiji/ImageJ free hand tool on images obtained Zeiss AXIO Zoom.V16
645 stereomicroscopy.
646
647 **Quantification of cell number**
648 Cell number was quantified using Fiji/ImageJ. To count the total cell and *esg-*
649 *GFP*$^{+}$ cell number, Hoechst and GFP signal was processed as following: (1)
650 despeckle, (2) binarization, (3) watershed, (4) analyze particle. The following cell
651 number was manually counted using the cell counter function: PH3^{+} cells,
652 *Su(H)GBE-lacZ*$^{+}$ cells, and Fly-Fucci^{+} cells.
653 For size quantification of MARCM clones, clones containing two or more
654 ISCs were selected, and the number of cells in the clone was counted manually.
655
656 **Quantification of signal intensity**
657 The signal intensity of reporter lines (*EGFP::BubR1*^{WT}*, GFP-Mad2*) was
658 quantified using Fiji/ImageJ. The signal areas were selected as ROIs using the
659 polygon selection tool. The reporter intensity in each ROI was quantified using
660 the Measure command.
661
662 **Statistics**
663 Statistical analyses were performed using Excel and RStudio. Two tailed *t* tests
664 were used for comparisons between two groups. One-way ANOVAs with post hoc
665 Tukey tests were performed when comparing three or more groups. Log-rank
666 tests were used for comparison of survival curve. Significance is indicated in the
667 figures as follows: $^{*}P \leq 0.05$, $^{**}P \leq 0.01$, $^{***}P \leq 0.001$, not significant
668 (N.S.): $P > 0.05$. Bar graphs show mean ± standard error. Boxplots show median
669 (thick line in the box), first and third quartiles (bottom and top of the box),
670 minimum value (lower whisker), and maximum value (upper whisker). Dots in bar
671 graphs and boxplots indicate individual values. Violin plots portray the distribution
672 of individual values.

673
674
675 ## Figure legends
676 **Figure 1. The adult midgut of *Drosophila* undergoes remodeling in**
677 **response to diapause and recovery**
678 (A) Schematic of diapause and its recovery in *D. melanogaster*. LD = Light : Dark.
679 (B) Representative images of the midgut under the 3 weeks diapause (3wD) and
680 recovery (3wD+R) condition. The two orange lines indicate anterior and posterior
681 end of the midgut. Scale bars: 1 mm.
682 (C, D) Quantification of the midgut length of the wild-type flies (Canton-S) under
683 diapause and control conditions (C) and their recovery conditions (D). *n*=10-15
684 midguts for each condition. The same diapause samples are quantified in (C) and
685 (D).
686 (E) Quantification of the midgut length and area in the anterior and posterior
687 region. Canton-S was analyzed. *n*=6 (3wC), 9 (3wD), and 21 (3wD+R) midguts
688 for length measurements and *n*=15 (3wC), 20 (3wD), 17(3wD+R) midguts for
689 area measurements.
690 (F) Quantification of the midgut length and area in the anterior and posterior
691 region. w^{1118} was analyzed. *n*=10 (3wC), 10 (3wD), 15 (3wD+R) midguts for length
692 measurements and *n*=10 (3wC), 11 (3wD), 15 (3wD+R) midguts for area
693 measurements.
694 (G) Female adult of *D. bifasciata* (JZK3) and *D. triauraria* (TM15-92). Scale bars:
695 1 mm.
696 (H) Schematic of diapause and its recover conditions in *D. bifasciata* and *D.*
697 *triauraria.* Light: Dark= 16 : 8 (hours) for long day (LD) condition, 10 : 14 (hours)
698 for short day (SD) condition.
699 (I) Representative images of the midgut in *D. bifasciata* (JZK3) under control (LD),
700 diapause (SD), and recover conditions. Scale bars: 1 mm.
701 (J, K) Quantification of the midgut length in *D. bifasciata* (J) and *D. triauraria* (K).
702 *n*=7-12 midguts for each condition.
703
704 **Figure 2. ISCs are in cell cycle arrest and inhibition of mitosis during**
705 **diapause**

706 (A, B) Schematics of the structure (A) and cell types (B) of the adult midgut of
707 *D. melanogaster*. Intestinal stem cell (ISC) generates an enteroblast (EB) or an
708 enteroendocrine progenitor (EEP), which differentiates into an enterocyte (EC)
709 or an enteroendocrine cell (EE).
710 (C) Total cell number in the adult midgut of wild-type flies under 3 weeks control
711 (3wC), 3 weeks diapause (3wD), and recovery after 3 weeks diapause (3wD+R).
712 *n*=7 (3wC), 8 (3wD), 8 (3wD+R) midguts.
713 (D) Representative images of *esg-GFP*$^{+}$ cells in the posterior midgut under 3wC
714 and 3wD conditions. Scale bars: 100 μm.
715 (E) Quantification of *esg-GFP*$^{+}$ cell number. *n*=11 (3wC),12 (3wD),10 (3wD+R)
716 midguts.
717 (F) Representative images of anti-PH3 staining in 3wC and 3wD wild-type flies.
718 Scale bars: 100 μm.
719 (G) PH3+ cell number in the anterior and posterior regions of 3wC and 3wD flies.
720 *n*=6 (3wC), 8 (3wD) midguts.
721 (H) Schematics of MARCM clone induction. ISC was labeled before eclosion, and
722 clonal expansion was examined at 1 week after eclosion.
723 (I) Representative images of MARCM clones in 1wC and 1wD conditions. A single
724 clone derived from an ISC is enclosed within the orange lines. Scale bars: 50 μm.
725 (J) Quantification of clone size. *n*=21 (1wC),10 (1wD) clones.
726 (K)(L) Representative images of the Fly-Fucci signals in the progenitor (esg+)
727 cells. Scale bars: 100 μm. The proportion of G2/M (GFP+ and RFP+ cells) is
728 higher under the 3wD condition. *n*=7 (3wC), 5 (3wD) midguts.
729
730
731 **Figure 3. BubR1 expression increases in the cytoplasm of ISCs during**
732 **diapause**
733 (A) MA plot of differentially expressed genes in a pair-wise comparison of
734 between 3wC and 3wD conditions.
735 (B, C) Gene ontology (GO) enrichment for upregulated genes (B) and
736 downregulated genes (C) in 3wD.
737 (D) Cell-cycle-related GO terms (biological process, BP) enriched in 3wD (left)
738 and heat map of “cell cycle checkpoint signaling" genes (right). These GO terms

739 were identified through enrichment analysis of all differentially expressed genes.
740 (E) Expression level of *BubR1* in 3wC and 3wD midguts. RNA-seq data were
741 used to examine the expression level. Count data was normalized with RLE
742 (Relative Log Expression). *n*=4 (3wC), 4 (3wD) RNA samples.
743 (F) Representative images of EGFP::BubR1 in the midgut under 3wC and 3wD
744 conditions. Scale bars: 50 μm.
745 (G) Quantification of the EGFP::BubR1 signal intensity of (F). 30 cells from 4
746 midguts (3wC), 41 cells from 4 midguts (3wD).
747 (H) Representative images of BubR1 localization in ISCs. BubR1 is localized in
748 the cytosol under the 3wD condition while BubR1 is accumulated at the
749 kinetochore (KT) after colchicine treatment. Scale bars: 10 μm.
750 (I) The proportion of BubR1 localization in mitotic (PH3+) cells. 215 cells from 6
751 midguts (3wD), 31 cells from 4 midguts (Colchicine feeding fly).
752
753 **Figure 4. BubR1 expression in ISCs is essential for DDMR**
754 (A) RT-qPCR of *BubR1* in control and *BubR1* heterozygous mutant flies under
755 the 3wC and 3wD condition. *n*=4 (3wC, w^{1118}), 3 (3wC, $BubR1^{k06109}$/+), 4 (3wC,
756 $BubR1^{k03113}$/+), 4 (3wD, w^{1118}), 4 (3wD, $BubR1^{k06109}$/+), 4 (3wD, $BubR1^{k03113}$/+)
757 RNA samples.
758 (B) Representative images of the midgut in control and *BubR1* heterozygous
759 mutant flies under the 3wD conditions. Scale bars: 1 mm.
760 (C) Quantification of the midgut length in control, *BubR1* heterozygous mutant,
761 and $EGFP::BubR1^{WT}$ flies under 3wD. In $EGFP::BubR1^{WT}$ flies, wild-type form of
762 *BubR1* is BAC rescued in the *BubR1* trans-heterozygous mutant background.
763 *n*=27 (w^{1118}), 22 ($BubR1^{k06109}$/+), 18 ($BubR1^{k03113}$/+), 23 ($EGFP::BubR1^{WT}$)
764 midguts.
765 (D) Total cell number in control, *BubR1* heterozygous mutants, and
766 $EGFP::BubR1^{WT}$ rescue flies under 3wD. *n*=10 (w^{1118}), 10 ($BubR1^{k06109}$/+), 15
767 ($BubR1^{k03113}$/+), 23 ($EGFP::BubR1^{WT}$) midguts.
768 (E) PH3+ cell number in control, *BubR1* heterozygous mutants, and
769 $EGFP::BubR1^{WT}$ rescue flies under 3wD. *n*=16 (w^{1118}), 10 ($BubR1^{k06109}$/+), 15
770 ($BubR1^{k03113}$/+), 22 ($EGFP::BubR1^{WT}$) midguts.
771 (F) Quantification of *esg*+ cell number in control, *BubR1* heterozygous mutants

772 under 3wD. *n*=23 (w^{1118}), 11 ($BubR1^{k06109}$/+), 16 ($BubR1^{k03113}$/+) midguts.
773 (G) Schematic of CRISPR-mediated *BubR1* knockout in *esg*+ cells.
774 (H) Quantification of the midgut length in control and *esg*+-specific *BubR1*
775 knockout flies. *n*=10 (esg^{Cas9}>+),10 (esg^{Cas9}>$BubR1^{CRISPR}$) midguts.
776 (I) Total cell number in control and *esg*+-specific *BubR1* knockout flies. *n*=9
777 (esg^{Cas9}>+),9 (esg^{Cas9}>$BubR1^{CRISPR}$) midguts.
778 (J) PH3+ cell number in control and *esg*+-specific *BubR1* knockout flies. *n*=10
779 (esg^{Cas9}>+),10 (esg^{Cas9}>$BubR1^{CRISPR}$) midguts.
780
781 **Figure 5. The MCC component Mad2 is involved in DDMR**
782 (A) Expression level of *mad2* in 3wC and 3wD midguts. RNA-seq data were used
783 to examine the expression level. Count data was normalized with RLE.
784 (B) Representative images of *GFP-Mad2* midguts under 3wC and 3wD conditions.
785 (C) Quantification of GFP-Mad2 signal intensity of (B). 40 cells from 4 midguts
786 (3wC), 52 cells from 4 midguts (3wD).
787 (D) Representative images of the midgut in control and *mad2* heterozygous
788 mutant flies under 3wD. Scale bars: 1 mm.
789 (E) Quantification of the midgut length in control and *mad2* heterozygous mutant
790 flies under 3wD. *n*=12 (w^{1118}), 9 ($mad2^{\Delta}$/+), 7 ($mad2^{EY}$/+) midguts. Same w^{1118}
791 control samples were used in Figure 5E and Figure 4C.
792 (F) Quantification of *esg*+ cell number in control and *mad2* heterozygous mutant
793 flies under 3wD. *n*=23 (w^{1118}), 10 ($mad2^{\Delta}$/+), 6 ($mad2^{EY}$/+) midguts. The w^{1118}
794 control are same sample with Figure 4E.
795 (G) Starvation resistance in control and *BubR1* heterozygous mutant flies. *n*=128
796 (w^{1118}), 114 ($BubR1^{k06109}$/+), 103 ($BubR1^{k03113}$/+) flies.
797 (H) Graphical summary of midgut remodeling in diapause and recovery
798 conditions.
799
800 **Figure S1. Midgut remodeling in coordination with *Drosophila* reproductive**
801 **diapause**
802 (A) Representative picture of ovary growth arrest in *D. melanogaster* diapause.
803 Scale bar: 1 mm.
804 (B) Schematic of control and its recovery in *D. melanogaster*. LD = Light : Dark.

805 (C) Quantification of the midgut length of the wild-type flies (Canton-S) under
806 control conditions and their recovery conditions. *n*=6-13 midguts for each
807 condition. The control samples are same with Figure 1C.
808 (D) Quantification of the midgut length in recovery condition for 1-7 days. *n*=8-21
809 midguts for each condition.
810 (E) Schematic of diapause and cold condition in *D. melanogaster*. LD = Light :
811 Dark. To set up cold condition, we allowed the flies to grow in 18°C for 4 days
812 after eclosion, and then subjected them to 10 °C and 8 L:16D photoperiods for 3
813 weeks.
814 (F) Quantification of the midgut length under diapause and cold condition in 3
815 weeks. *n*=9-21 midguts for each condition. The 3 weeks diapause samples are
816 same with Figure 1C.
817 (G) Quantification of the midgut length and area in wild-type male flies (Canton-
818 S) under 3wC and 3wD condition. *n*=7 (3wC), 7 (3wD) midguts.
819 (H) Representative pictures of ovaries in *D. bifasciata* (JZK3) and *D. triauraria*
820 (TM15-92) under the long day (LD) and short day (SD) conditions. In SD, ovarian
821 growth arrest was induced. Scale bars: 1 mm.
822 (I, J) Quantification of the midgut length of non-diapause strains of *D. triauraria*
823 (KMJ1 and OEB12) under LD and SD conditions. *n*=11 (KMJ1, LD), 11 (KMJ1,
824 SD), 8 (OEB12, LD), 13 (OEB12, SD) midguts. KMJ1 and OEB12 female flies do
825 not enter diapause state in SD condition (Yamada & Yamamoto, 2011).
826
827 **Figure S2. ISCs remain in a non-proliferative state during diapause**
828 (A) The proportion of esg+ cells in total cells. *n*=11 (3wC), 12 (3wD), 10 (3wD+R)
829 midguts.
830 (B) Representative images of the posterior midgut under 3wC and 3wD
831 conditions in *Dl-lacZ* flies. Scale bars: 100 μm.
832 (C) Representative images of anti-Dl staining in 3wC and 3wD wild-type flies.
833 Scale bars: 100 μm.
834 (D) Representative images of the posterior midgut under 3wC and 3wD
835 conditions in *Su(H)GBE-lacZ* flies. Scale bars: 100 μm.
836 (E) Quantification of the Su(H)+ cell number. *n*=8 (3wC), 6 (3wD) midguts.
837 (F) The proportion of Su(H)+ cells in total cells. *n*=8 (3wC), 6 (3wD) midguts.

838 (G) PH3+ cell number in the midgut of 3wC, 3wD, and 3wD+R flies. n=6 (3wC),
839 8 (3wD), 6 (3wD+R) midguts. The 3wC and 3wD samples are same with Figure
840 2F.
841 (H) Representative images of the posterior midgut under 3wC and 3wD
842 conditions in *CycB-GFP* flies. Scale bars: 100 μm.
843 (I) Representative images of anti-cDcp1 staining in 3wC and 3wD wild-type flies.
844 Scale bars: 50 μm.
845
846 **Figure S3. Molecular signatures identified by RNA-seq analysis in DDMR**
847 (A) Gene ontology (GO) enrichment of transcriptome in 3wD compared to 3wC..
848 All differentially expressed genes in 3wD are used for enrichment analysis.
849 (B) Reactome Pathway Enrichment in 3wD compared to 3wC. All differentially
850 expressed genes in 3wD are used for enrichment analysis.
851 (C) Expression level of *bmm, pepck, tobi* from RNA-seq data. *n*=4 (3wC), 4 (3wD)
852 RNA samples. Count data was normalized with RLE.
853 (D) Expression level of *per, tim* from RNA-seq data. *n*=4 (3wC), 4 (3wD) RNA
854 samples. Count data was normalized with RLE.
855 (E) Expression level of *Drs* from RNA-seq data. *n*=4 (3wC), 4 (3wD) RNA samples.
856 Count data was normalized with RLE.
857 (F) Representative images of GFP-BubR1 of the posterior midgut under 3wC and
858 3wD. Scale bar: 100 μm.
859 (G) MA plot of differentially expressed genes in a pair-wise comparison of
860 3wC+R and 3wD+R condition.
861 (H) Gene ontology (GO) enrichment in 3wD+R compared to 3wC+R. All
862 differentially expressed genes in 3wD+R are used for enrichment analysis.
863 (I) Reactome Pathway Enrichment in 3wD+R compared to 3wC+R. All
864 differentially expressed genes in 3wD+R are used for enrichment analysis.
865 (J) Expression level of *CCHa2, Dh31, dilp3, NPF, Thor* from RNA-seq data. *n*=4
866 (3wC+R), 4 (3wD+R) RNA samples. Count data was normalized with RLE.
867
868 **Figure S4. BubR1 functions in the midgut in coordination with *Drosophila***
869 **reproductive diapause**
870 (A) Quantification of the midgut length in control and *BubR1* heterozygous mutant

under 3wC. *n*=10 (w^{1118}), 8 ($BubR1^{k06109}$/+), 8 ($BubR1^{k03113}$/+) midguts.

(B) PH3+ cell number in control, *BubR1* heterozygous mutants, and *EGFP::BubR1*^{WT} flies under 3wC. *n*=10 (w^{1118}), 8 ($BubR1^{k06109}$/+), 8 ($BubR1^{k03113}$/+) midguts.

(C) RT-qPCR of *BubR1* in control and CRISPR-mediated *BubR1* knockout flies under the 3wD condition. *n*=9 (esg^{Cas9}>+), 9 (esg^{Cas9}>$BubR1^{CRISPR}$) RNA samples.

(D) RT-qPCR of *BubR1* in *D. bifasciata* (JZK3) midgut under the control (LD) and diapause (SD) condition. *n*=8 (LD), 9 (SD) RNA samples.

(E) RT-qPCR of *BubR1* in *D. triauraria* (TM15-92) midgut under the control (LD) and diapause (SD) condition. *n*=6 (LD), 8 (SD) RNA samples.

References

Anduaga, A. M., Nagy, D., Costa, R., & Kyriacou, C. P. (2018). Diapause in Drosophila melanogaster – Photoperiodicity, cold tolerance and metabolites. *Journal of Insect Physiology*, *105*, 46–53. https://doi.org/10.1016/j.jinsphys.2018.01.003

Baker, D. J., Dawlaty, M. M., Wijshake, T., Jeganathan, K. B., Malureanu, L., Van Ree, J. H., Crespo-Diaz, R., Reyes, S., Seaburg, L., Shapiro, V., Behfar, A., Terzic, A., Van De Sluis, B., & Van Deursen, J. M. (2013). Increased expression of BubR1 protects against aneuploidy and cancer and extends healthy lifespan. *Nature Cell Biology*, *15*(1), 96–102. https://doi.org/10.1038/ncb2643

Baker, D. J., Jeganathan, K. B., Cameron, J. D., Thompson, M., Juneja, S., Kopecka, A., Kumar, R., Jenkins, R. B., De Groen, P. C., Roche, P., & Van Deursen, J. M. (2004). BubR1 insufficiency causes early onset of aging-associated phenotypes and infertility in mice. *Nature Genetics*, *36*(7), 744–749. https://doi.org/10.1038/ng1382

Bellen, H. J., Levis, R. W., He, Y., Carlson, J. W., Evans-Holm, M., Bae, E., Kim, J., Metaxakis, A., Savakis, C., Schulze, K. L., Hoskins, R. A., & Spradling, A. C. (2011). The Drosophila gene disruption project: Progress using

transposons with distinctive site specificities. *Genetics*, *188*(3), 731–743. https://doi.org/10.1534/genetics.111.126995

Bier, E., Harrison, M. M., O'connor-Giles, K. M., & Wildonger, J. (2018). Advances in engineering the fly genome with the CRISPR-Cas system. *Genetics*, *208*(1), 1–18. https://doi.org/10.1534/genetics.117.1113

Buchon, N., Osman, D., David, F. P. A., Yu Fang, H., Boquete, J. P., Deplancke, B., & Lemaitre, B. (2013). Morphological and Molecular Characterization of Adult Midgut Compartmentalization in Drosophila. *Cell Reports*, *3*(5), 1725–1738. https://doi.org/10.1016/j.celrep.2013.04.001

Buffin, E., Emre, D., & Karess, R. E. (2007). Flies without a spindle checkpoint. *Nature Cell Biology*, *9*(5), 565–572. https://doi.org/10.1038/ncb1570

Buffin, E., Lefebvre, C., Huang, J., Gagou, M. E., & Karess, R. E. (2005). Recruitment of Mad2 to the Kinetochore Requires the Rod/Zw10 Complex. *Current Biology*, *15*(9), 856–861. https://doi.org/10.1016/j.cub.2005.03.052

Choi, E., Zhang, X., Xing, C., & Yu, H. (2016). Mitotic Checkpoint Regulators Control Insulin Signaling and Metabolic Homeostasis. *Cell*, *166*(3), 567–581. https://doi.org/10.1016/j.cell.2016.05.074

Christensen, C. F., Laurichesse, Q., Loudhaief, R., Colombani, J., & Andersen, D. S. (2024). Drosophila activins adapt gut size to food intake and promote regenerative growth. *Nature Communications*, *15*(1), 273. https://doi.org/10.1038/s41467-023-44553-9

Denlinger, D. L. (2022). *Insect Diapause* (Vol. 464). Cambridge University Press. https://doi.org/10.1017/9781108609364

DiVito Evans, A., Fairbanks, R. A., Schmidt, P., & Levine, M. T. (2023). Histone methylation regulates reproductive diapause in Drosophila melanogaster. *PLOS Genetics*, *19*(9), e1010906. https://doi.org/10.1371/journal.pgen.1010906

Easwaran, S., & Montell, D. J. (2023). The molecular mechanisms of diapause and diapause-like reversible arrest. In *Biochemical Society Transactions* (Vol. 51, Issue 5, pp. 1847–1856). Portland Press Ltd. https://doi.org/10.1042/BST20221431

Easwaran, S., & Montell, D. J. (2024). *A genome-wide association study implicates the olfactory system in Drosophila melanogaster diapause-*

associated lifespan extension and fecundity. https://doi.org/10.7554/eLife.98142.2

Easwaran, S., Van Ligten, M., Kui, M., & Montell, D. J. (2022). Enhanced germline stem cell longevity in Drosophila diapause. *Nature Communications*, *13*(1). https://doi.org/10.1038/s41467-022-28347-z

Fang, Y., Liu, T., Wang, X., Yang, Y. M., Deng, H., Kunicki, J., Traganos, F., Darzynkiewicz, Z., Lu, L., & Dai, W. (2006). BubR1 is involved in regulation of DNA damage responses. *Oncogene*, *25*(25), 3598–3605. https://doi.org/10.1038/sj.onc.1209392

Goto, S., & Hayashi, S. (1999). Proximal to distal cell communication in the *Drosophila* leg provides a basis for an intercalary mechanism of limb patterning. *Development*, *126*(15), 3407–3413. https://doi.org/10.1242/dev.126.15.3407

Gray, D. R., Logan, J. A., Ravlin, F. W., & Carlson, J. A. (1991). Toward a Model of Gypsy Moth Egg Phenology: Using Respiration Rates of Individual Eggs to Determine Temperature–Time Requirements of Prediapause Development. *Environmental Entomology*, *20*(6), 1645–1652. https://doi.org/10.1093/ee/20.6.1645

Guo, Z., Driver, I., & Ohlstein, B. (2013). Injury-induced BMP signaling negatively regulates *Drosophila* midgut homeostasis. *Journal of Cell Biology*, *201*(6), 945–961. https://doi.org/10.1083/jcb.201302049

Guo, Z., & Ohlstein, B. (2015). Bidirectional Notch signaling regulates Drosophila intestinal stem cell multipotency. *Science*, *350*(6263), 927. https://doi.org/10.1126/science.aab0988

Hara, Y., & Yamamoto, D. (2022). Effects of Food and Temperature on Drosophila melanogaster Reproductive Dormancy as Revealed by Quantification of a GFP-Tagged Yolk Protein in the Ovary. *Frontiers in Physiology*, *12*. https://doi.org/10.3389/fphys.2021.803144

Harsimran Kaur Gill, Gaurav Goyal, & Gurminder Chahil. (2017). Insect Diapause: A Review. *Journal of Agricultural Science and Technology A*, *7*(7). https://doi.org/10.17265/2161-6256/2017.07.002

Helfrich-Förster, C. (2024). Neuropeptidergic regulation of insect diapause by the circadian clock. In *Current Opinion in Insect Science* (Vol. 63). Elsevier Inc.

https://doi.org/10.1016/j.cois.2024.101198

Huang, J.-Y., & Raff, J. W. (1999). The disappearance of cyclin B at the end of mitosis is regulated spatially in Drosophila cells. In *The EMBO Journal* (Vol. 18, Issue 8). https://www.embopress.org

Hung, R.-J., Hu, Y., Kirchner, R., Liu, Y., Xu, C., Comjean, A., Tattikota, S. G., Li, F., Song, W., Ho Sui, S., & Perrimon, N. (2020). A cell atlas of the adult *Drosophila* midgut. *Proceedings of the National Academy of Sciences*, *117*(3), 1514–1523. https://doi.org/10.1073/pnas.1916820117

Karess, R. E., Wassmann, K., & Rahmani, Z. (2013). New insights into the role of BubR1 in mitosis and beyond. In *International Review of Cell and Molecular Biology* (Vol. 306, pp. 223–273). Elsevier Inc. https://doi.org/10.1016/B978-0-12-407694-5.00006-7

Karp, X. (2021). Hormonal Regulation of Diapause and Development in Nematodes, Insects, and Fishes. In *Frontiers in Ecology and Evolution* (Vol. 9). Frontiers Media S.A. https://doi.org/10.3389/fevo.2021.735924

Kim, M., & Denlinger, D. L. (2009). Decrease in expression of beta-tubulin and microtubule abundance in flight muscles during diapause in adults of Culex pipiens. *Insect Molecular Biology*, *18*(3), 295–302. https://doi.org/10.1111/j.1365-2583.2009.00870.x

Kim, M., Robich, R. M., Rinehart, J. P., & Denlinger, D. L. (2006). Upregulation of two actin genes and redistribution of actin during diapause and cold stress in the northern house mosquito, Culex pipiens. *Journal of Insect Physiology*, *52*(11–12), 1226–1233. https://doi.org/10.1016/j.jinsphys.2006.09.007

Kimura, M. T. (1990). Quantitative response to photoperiod during reproductive diapause in the Drosophila auraria species-complex. *Journal of Insect Physiology*, *36*(3), 147–152. https://doi.org/10.1016/0022-1910(90)90115-V

Kubrak, O. I., Kučerová, L., Theopold, U., & Nässel, D. R. (2014). The sleeping beauty: How reproductive diapause affects hormone signaling, metabolism, immune response and somatic maintenance in Drosophila melanogaster. *PLoS ONE*, *9*(11). https://doi.org/10.1371/journal.pone.0113051

Kubrak, O. I., Kucerová, L., Theopold, U., Nylin, S., & Nässel, D. R. (2016). Characterization of reproductive dormancy in male Drosophila melanogaster. *Frontiers in Physiology*, *7*(NOV). https://doi.org/10.3389/fphys.2016.00572

Kučerová, L., Kubrak, O. I., Bengtsson, J. M., Strnad, H., Nylin, S., Theopold, U., & Nässel, D. R. (2016). Slowed aging during reproductive dormancy is reflected in genome-wide transcriptome changes in Drosophila melanogaster. *BMC Genomics*, *17*(1). https://doi.org/10.1186/s12864-016-2383-1

Kurogi, Y., Imura, E., Mizuno, Y., Hoshino, R., Nouzova, M., Matsuyama, S., Mizoguchi, A., Kondo, S., Tanimoto, H., Noriega, F. G., & Niwa, R. (2023). Female reproductive dormancy in Drosophila is regulated by DH31-producing neurons projecting into the corpus allatum. *Development (Cambridge, England)*, *150*(10). https://doi.org/10.1242/dev.201186

Kurtz, C. C., Otis, J. P., Regan, M. D., & Carey, H. V. (2021). How the gut and liver hibernate. In *Comparative Biochemistry and Physiology -Part A : Molecular and Integrative Physiology* (Vol. 253). Elsevier Inc. https://doi.org/10.1016/j.cbpa.2020.110875

LAKOVAARA, S., SAURA, A., KOREF-SANTIBAÑEZ, S., & EHRMAN, L. E. E. (1972). Aspects of diapause and its genetics in northern drosophilids. *Hereditas*, *70*(1), 89–96. https://doi.org/https://doi.org/10.1111/j.1601-5223.1972.tb00996.x

Le Bras, S., & Van Doren, M. (2006). Development of the male germline stem cell niche in Drosophila. *Developmental Biology*, *294*(1), 92–103. https://doi.org/10.1016/j.ydbio.2006.02.030

Li, H., & Jasper, H. (2016). Gastrointestinal stem cells in health and disease: from flies to humans. *Disease Models & Mechanisms*, *9*(5), 487–499. https://doi.org/10.1242/dmm.024232

Lirakis, M., Dolezal, M., & Schlötterer, C. (2018). Redefining reproductive dormancy in Drosophila as a general stress response to cold temperatures. *Journal of Insect Physiology*, *107*, 175–185. https://doi.org/10.1016/j.jinsphys.2018.04.006

Liu, M., Yang, S., Yang, J., Feng, P., Luo, F., Zhang, Q., Yang, L., & Jiang, H. (2024). BubR1 controls starvation-induced lipolysis via IMD signaling pathway in Drosophila. *Aging*, *16*(4), 3257–3279. https://doi.org/10.18632/aging.205533

Malita, A., Kubrak, O., Koyama, T., Ahrentløv, N., Texada, M. J., Nagy, S., Halberg,

K. V., & Rewitz, K. (2022). A gut-derived hormone suppresses sugar appetite and regulates food choice in Drosophila. *Nature Metabolism*, *4*(11), 1532–1550. https://doi.org/10.1038/s42255-022-00672-z

Marianes, A., & Spradling, A. C. (2013). Physiological and stem cell compartmentalization within the Drosophila midgut. *ELife*, *2*. https://doi.org/10.7554/eLife.00886

Mattila, J., Viitanen, A., Fabris, G., Strutynska, T., Korzelius, J., & Hietakangas, V. (2024). Stem cell mTOR signaling directs region-specific cell fate decisions during intestinal nutrient adaptation. *Science Advances*, *10*(6). https://doi.org/10.1126/sciadv.adi2671

McGuire, S. E., Le, P. T., Osborn, A. J., Matsumoto, K., & Davis, R. L. (2003). Spatiotemporal Rescue of Memory Dysfunction in *Drosophila*. *Science*, *302*(5651), 1765–1768. https://doi.org/10.1126/science.1089035

Meiselman, M. R., Alpert, M. H., Cui, X., Shea, J., Gregg, I., Gallio, M., & Yapici, N. (2022). Recovery from cold-induced reproductive dormancy is regulated by temperature-dependent AstC signaling. *Current Biology*, *32*(6), 1362-1375.e8. https://doi.org/10.1016/j.cub.2022.01.061

Meller, C. L., Meller, R., Simon, R. P., Culpepper, K. M., Podrabsky, J. E., Meller, C., Lynn, ;, Meller, R. ;, Simon, R. P. ;, & Culpepper, K. M. ; (2012). Cell Cycle Arrest Associated with Anoxia-Induced Quiescence, Anoxic Preconditioning, and Embryonic Diapause in Embryos of the Annual Killifish Austrofundulus Limnaeus Citation Details. In *Biology Faculty Publications and Presentations Biology*. https://pdxscholar.library.pdx.edu/bio_fac/47

Meltzer, H., Marom, E., Alyagor, I., Mayseless, O., Berkun, V., Segal-Gilboa, N., Unger, T., Luginbuhl, D., & Schuldiner, O. (2019). Tissue-specific (ts)CRISPR as an efficient strategy for in vivo screening in Drosophila. *Nature Communications*, *10*(1), 2113. https://doi.org/10.1038/s41467-019-10140-0

Meyerhof, G. T., Easwaran, S., Bontempo, A. E., Montell, C., & Montell, D. J. (2024). Altered circadian rhythm, sleep, and *rhodopsin 7* –dependent shade preference during diapause in *Drosophila melanogaster*. *Proceedings of the National Academy of Sciences*, *121*(27). https://doi.org/10.1073/pnas.2400964121

Miguel-Aliaga, I., Jasper, H., & Lemaitre, B. (2018). Anatomy and Physiology of

the Digestive Tract of *Drosophila melanogaster*. *Genetics*, *210*(2), 357–396. https://doi.org/10.1534/genetics.118.300224

Musacchio, A. (2015). The Molecular Biology of Spindle Assembly Checkpoint Signaling Dynamics. In *Current Biology* (Vol. 25, Issue 20, pp. R1002–R1018). Cell Press. https://doi.org/10.1016/j.cub.2015.08.051

Nagai, H., Miura, M., & Nakajima, Y. ichiro. (2022). Cellular mechanisms underlying adult tissue plasticity in Drosophila. In *Fly* (Vol. 16, Issue 1, pp. 190–206). Taylor and Francis Ltd. https://doi.org/10.1080/19336934.2022.2066952

Nagai, H., Nagai, L. A. E., Tasaki, S., Nakato, R., Umetsu, D., Kuranaga, E., Miura, M., & Nakajima, Y. (2023). Nutrient-driven dedifferentiation of enteroendocrine cells promotes adaptive intestinal growth in Drosophila. *Developmental Cell*, *58*(18), 1764-1781.e10. https://doi.org/10.1016/j.devcel.2023.08.022

Nakagaki, M., Takei, R., Nagashima, E., & Yaginuma, T. (1991). Cell cycles in embryos of the silkworm, Bombyx mori: G2-arrest at diapause .stage. In *Arch Dev Biol* (Vol. 200).

O'Brien, L. E., Soliman, S. S., Li, X., & Bilder, D. (2011). Altered modes of stem cell division drive adaptive intestinal growth. *Cell*, *147*(3), 603–614. https://doi.org/10.1016/j.cell.2011.08.048

Ojima, N., Hara, Y., Ito, H., & Yamamoto, D. (2018). Genetic dissection of stress-induced reproductive arrest in Drosophila melanogaster females. *PLoS Genetics*, *14*(6). https://doi.org/10.1371/journal.pgen.1007434

Park, J., Hall, C., Hubbard, B., LaMoia, T., Gaspar, R., Nasiri, A., Li, F., Zhang, H., Kim, J., Haeusler, R. A., Accili, D., Shulman, G. I., Yu, H., & Choi, E. (2023). MAD2-Dependent Insulin Receptor Endocytosis Regulates Metabolic Homeostasis. *Diabetes*, *72*(12), 1781–1794. https://doi.org/10.2337/db23-0314

Patro, R., Duggal, G., Love, M. I., Irizarry, R. A., & Kingsford, C. (2017). Salmon provides fast and bias-aware quantification of transcript expression. *Nature Methods*, *14*(4), 417–419. https://doi.org/10.1038/nmeth.4197

Reiff, T., Jacobson, J., Cognigni, P., Antonello, Z., Ballesta, E., Tan, K. J., Yew, J. Y., Dominguez, M., & Miguel-Aliaga, I. (2015). Endocrine remodelling of the

adult intestine sustains reproduction in Drosophila. *ELife*, *4*. https://doi.org/10.7554/eLife.06930

Resende, L. P., Monteiro, A., Brás, R., Lopes, T., & Sunkel, C. E. (2018). Aneuploidy in intestinal stem cells promotes gut dysplasia in Drosophila. *Journal of Cell Biology*, *217*(11), 3930–3946. https://doi.org/10.1083/jcb.201804205

Röttgen, G., Wagner, T., & Hinz, U. (1998). A genetic screen for elements of the network that regulates neurogenesis in Drosophila. *Molecular and General Genetics MGG*, *257*(4), 442–451. https://doi.org/10.1007/s004380050668

Saunders, D. S., Henricht, V. C., & Gilbertt, L. I. (1989). Induction of diapause in Drosophila melanogaster: Photoperiodic regulation and the impact of arrhythmic clock mutations on time measurement (ovarian diapause). In *Genetics* (Vol. 86).

Saunders, D. S., Richard, D. S., Applebaum, S. W., Ma, M., & Gilbert~, L. I. (1990). Photoperiodic Diapause in Drosophila melanogaster Involves a Block to the Juvenile Hormone Regulation of Ovarian Maturation. In *GENERAL AND COMPARATIVE ENDOCRINOLOGY* (Vol. 79).

Schiesari, L., Andreatta, G., Kyriacou, C. P., O'Connor, M. B., & Costa, R. (2016). The insulin-like proteins dILPs-2/5 determine diapause inducibility in Drosophila. *PLoS ONE*, *11*(9). https://doi.org/10.1371/journal.pone.0163680

Schiesari, L., & O'Connor, M. B. (2013). *Diapause* (pp. 213–246). https://doi.org/10.1016/B978-0-12-396968-2.00008-7

Shinoda, N., Horikoshi, M., Taira, Y., Muramoto, M., Hirayama, S., Murata, S., & Miura, M. (2023). Caspase cleaves Drosophila BubR1 to modulate spindle assembly checkpoint function and lifespan of the organism. *FEBS Journal*, *290*(17), 4200–4223. https://doi.org/10.1111/febs.16811

Soneson, C., Love, M. I., & Robinson, M. D. (2015). Differential analyses for RNA-seq: transcript-level estimates improve gene-level inferences. *F1000Research*, *4*, 1521. https://doi.org/10.12688/f1000research.7563.2

Song, Y.-H. (2005). Drosophila melanogaster: a model for the study of DNA damage checkpoint response. *Molecules and Cells*, *19*(2), 167–179.

Staples, J. F. (2016). Metabolic Flexibility: Hibernation, Torpor, and Estivation. In *Comprehensive Physiology* (pp. 737–771). Wiley.

https://doi.org/10.1002/cphy.c140064

Stojanović, O., Miguel-Aliaga, I., & Trajkovski, M. (2022). Intestinal plasticity and metabolism as regulators of organismal energy homeostasis. *Nature Metabolism*, *4*(11), 1444–1458. https://doi.org/10.1038/s42255-022-00679-6

Tammariello, S. P., & Denlinger, D. L. (1998). G0/G1 Cell Cycle Arrest in the Brain of Sarcophaga crassipalpis During Pupal Diapause and the Expression Pattern of the Cell Cycle Regulator, Proliferating Cell Nuclear Antigen. In *Insect Biochem. Molec. Biol* (Vol. 28, Issue 2).

Tang, R., Jiang, Z., Chen, F., Yu, W., Fan, K., Tan, J., Zhang, Z., Liu, X., Li, P., & Yuan, K. (2020). The Kinase Activity of Drosophila BubR1 Is Required for Insulin Signaling-Dependent Stem Cell Maintenance. *Cell Reports*, *31*(12), 107794. https://doi.org/10.1016/j.celrep.2020.107794

Tatar, M., & Yin, C.-M. (2001). Slow aging during insect reproductive diapause: why butterflies, grasshoppers and flies are like worms. *Experimental Gerontology*, *36*(4–6), 723–738. https://doi.org/10.1016/S0531-5565(00)00238-2

Trivedi, D., Vinitha, C. M., Bisht, K., Janardan, V., Pandit, A., Basak, B., Shwetha, H., Ramesh, N., & Raghu, P. (2020). A genome engineering resource to uncover principles of cellular organization and tissue architecture by lipid signaling. *ELife*, *9*, 1–23. https://doi.org/10.7554/ELIFE.55793

Watabe, H. (1979). *Drosophila Survey of Hokkaido, XXXVI. Seasonal Changes in the Reproductive Condition of Wild and Domestic Species of Drosophila*.

White, M. A., Bonfini, A., Wolfner, M. F., & Buchon, N. (2021). *Drosophila melanogaster* sex peptide regulates mated female midgut morphology and physiology. *Proceedings of the National Academy of Sciences*, *118*(1). https://doi.org/10.1073/pnas.2018112118

Wilsterman, K., Ballinger, M. A., & Williams, C. M. (2021). A unifying, eco-physiological framework for animal dormancy. *Functional Ecology*, *35*(1), 11–31. https://doi.org/10.1111/1365-2435.13718

Yamada, H., & Yamamoto, M. T. (2011). Association between circadian clock genes and diapause incidence in Drosophila triauraria. *PLoS ONE*, *6*(12). https://doi.org/10.1371/journal.pone.0027493

Yoshinari, Y., Nishimura, T., Yoshii, T., Kondo, S., Tanimoto, H., Kobayashi, T.,

Matsuyama, M., & Niwa, R. (2024). A high-protein diet-responsive gut hormone regulates behavioral and metabolic optimization in Drosophila melanogaster. *Nature Communications*, *15*(1), 10819. https://doi.org/10.1038/s41467-024-55050-y

Zhou, X., Ding, G., Li, J., Xiang, X., Rushworth, E., & Song, W. (2020). Physiological and Pathological Regulation of Peripheral Metabolism by Gut-Peptide Hormones in Drosophila. In *Frontiers in Physiology* (Vol. 11). Frontiers Media S.A. https://doi.org/10.3389/fphys.2020.577717

Zielke, N., Korzelius, J., vanStraaten, M., Bender, K., Schuhknecht, G. F. P., Dutta, D., Xiang, J., & Edgar, B. A. (2014). Fly-FUCCI: A Versatile Tool for Studying Cell Proliferation in Complex Tissues. *Cell Reports*, *7*(2), 588–598. https://doi.org/10.1016/j.celrep.2014.03.020

Figure 1

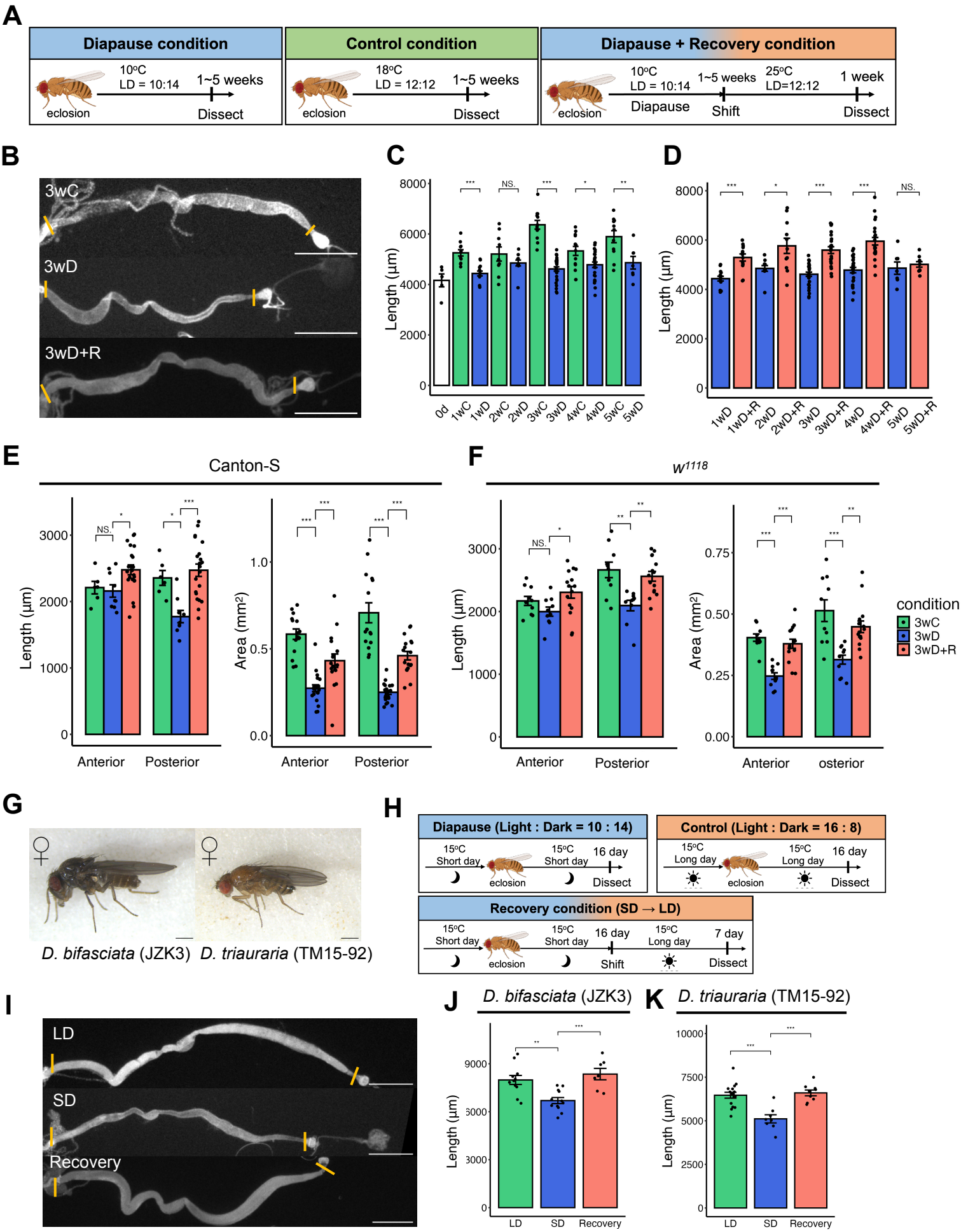
A
Diapause condition
10ºC
LD = 10:14
1~5 weeks
eclosion
Dissect
Control condition
18ºC
LD = 12:12
1~5 weeks
eclosion
Dissect
Diapause + Recovery condition
10ºC
LD = 10:14
1~5 weeks
25ºC
LD=12:12
1 week
eclosion
Diapause
Shift
Dissect
B
3wC
3wD
3wD+R
C
Length (µm)
0d
1wC
1wD
2wC
2wD
3wC
3wD
4wC
4wD
5wC
5wD
D
Length (µm)
1wD
1wD+R
2wD
2wD+R
3wD
3wD+R
4wD
4wD+R
5wD
5wD+R
E
Canton-S
Length (µm)
Area (mm²)
Anterior
Posterior
F
w1118
Length (µm)
Area (mm²)
Anterior
Posterior
osterior
condition
3wC
3wD
3wD+R
G
D. bifasciata (JZK3)
D. triauraria (TM15-92)
H
Diapause (Light : Dark = 10 : 14)
15ºC
Short day
eclosion
15ºC
Short day
16 day
Dissect
Control (Light : Dark = 16 : 8)
15ºC
Long day
eclosion
15ºC
Long day
16 day
Dissect
Recovery condition (SD → LD)
15ºC
Short day
eclosion
15ºC
Short day
16 day
Shift
15ºC
Long day
7 day
Dissect
I
LD
SD
Recovery
J
D. bifasciata (JZK3)
Length (µm)
LD
SD
Recovery
K
D. triauraria (TM15-92)
Length (µm)
LD
SD
Recovery

Figure 2

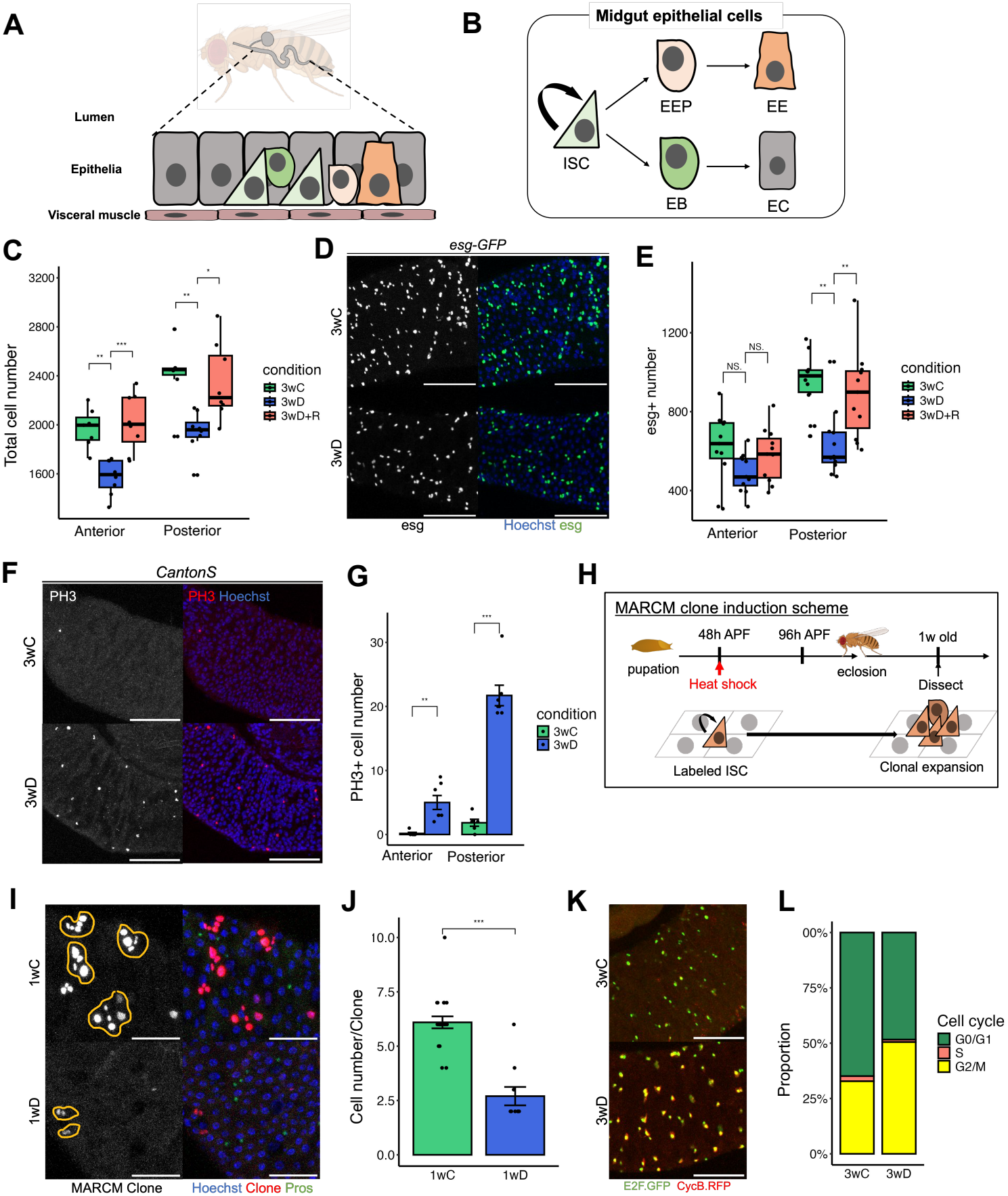
A
Lumen
Epithelia
Visceral muscle
B
Midgut epithelial cells
ISC
EEP
EE
EB
EC
C
Total cell number
condition
3wC
3wD
3wD+R
Anterior
Posterior
D
esg-GFP
3wC
3wD
esg
Hoechst esg
E
esg+ number
NS.
condition
3wC
3wD
3wD+R
Anterior
Posterior
F
CantonS
PH3
PH3 Hoechst
3wC
3wD
G
PH3+ cell number
condition
3wC
3wD
Anterior
Posterior
H
MARCM clone induction scheme
48h APF
96h APF
1w old
pupation
Heat shock
eclosion
Dissect
Labeled ISC
Clonal expansion
I
1wC
1wD
MARCM Clone
Hoechst Clone Pros
J
Cell number/Clone
1wC
1wD
K
3wC
3wD
E2F.GFP CycB.RFP
L
Proportion
Cell cycle
G0/G1
S
G2/M
3wC
3wD

Figure 3

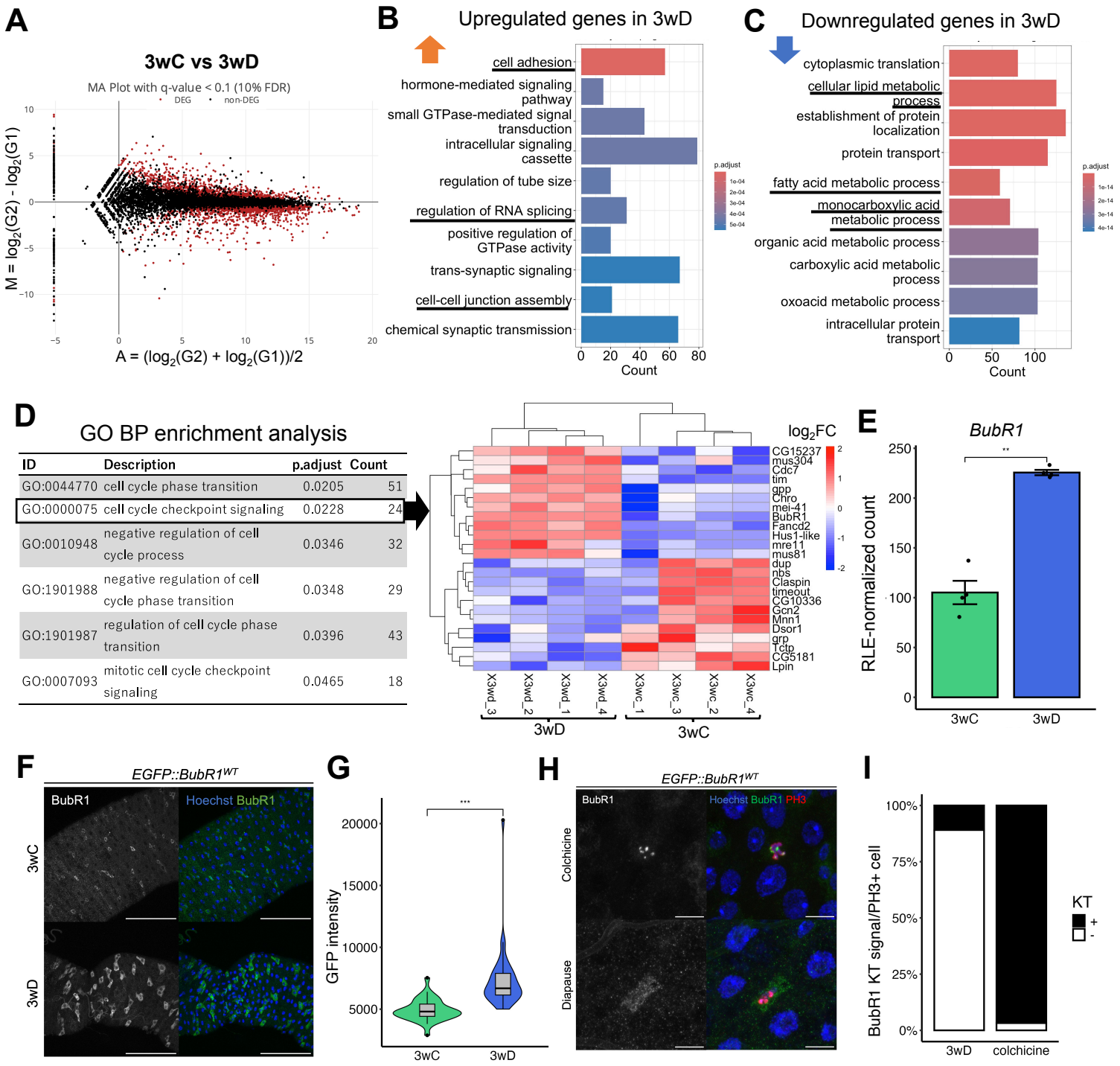
A
3wC vs 3wD
MA Plot with q-value < 0.1 (10% FDR)
DEG
non-DEG
M = log2(G2) - log2(G1)
A = (log2(G2) + log2(G1))/2
B
Upregulated genes in 3wD
cell adhesion
hormone-mediated signaling pathway
small GTPase-mediated signal transduction
intracellular signaling cassette
regulation of tube size
regulation of RNA splicing
positive regulation of GTPase activity
trans-synaptic signaling
cell-cell junction assembly
chemical synaptic transmission
Count
p.adjust
C
Downregulated genes in 3wD
cytoplasmic translation
cellular lipid metabolic process
establishment of protein localization
protein transport
fatty acid metabolic process
monocarboxylic acid metabolic process
organic acid metabolic process
carboxylic acid metabolic process
oxoacid metabolic process
intracellular protein transport
Count
p.adjust
D
GO BP enrichment analysis
ID Description p.adjust Count
GO:0044770 cell cycle phase transition 0.0205 51
GO:0000075 cell cycle checkpoint signaling 0.0228 24
GO:0010948 negative regulation of cell cycle process 0.0346 32
GO:1901988 negative regulation of cell cycle phase transition 0.0348 29
GO:1901987 regulation of cell cycle phase transition 0.0396 43
GO:0007093 mitotic cell cycle checkpoint signaling 0.0465 18
log2FC
CG15237
mus304
Cdc7
tim
gpp
Chro
mei-41
BubR1
Fancd2
Hus1-like
mre11
mus81
dup
nbs
Claspin
timeout
CG10336
Gcn2
Mnn1
Dsor1
grp
Tctp
CG5181
Lpin
X3wd_3
X3wd_2
X3wd_1
X3wd_4
X3wc_1
X3wc_3
X3wc_2
X3wc_4
3wD
3wC
E
BubR1
RLE-normalized count
3wC
3wD
F
EGFP::BubR1WT
BubR1
Hoechst BubR1
3wC
3wD
G
GFP intensity
3wC
3wD
H
EGFP::BubR1WT
BubR1
Hoechst BubR1 PH3
Colchicine
Diapause
I
BubR1 KT signal/PH3+ cell
KT
+
-
3wD
colchicine

Figure 4

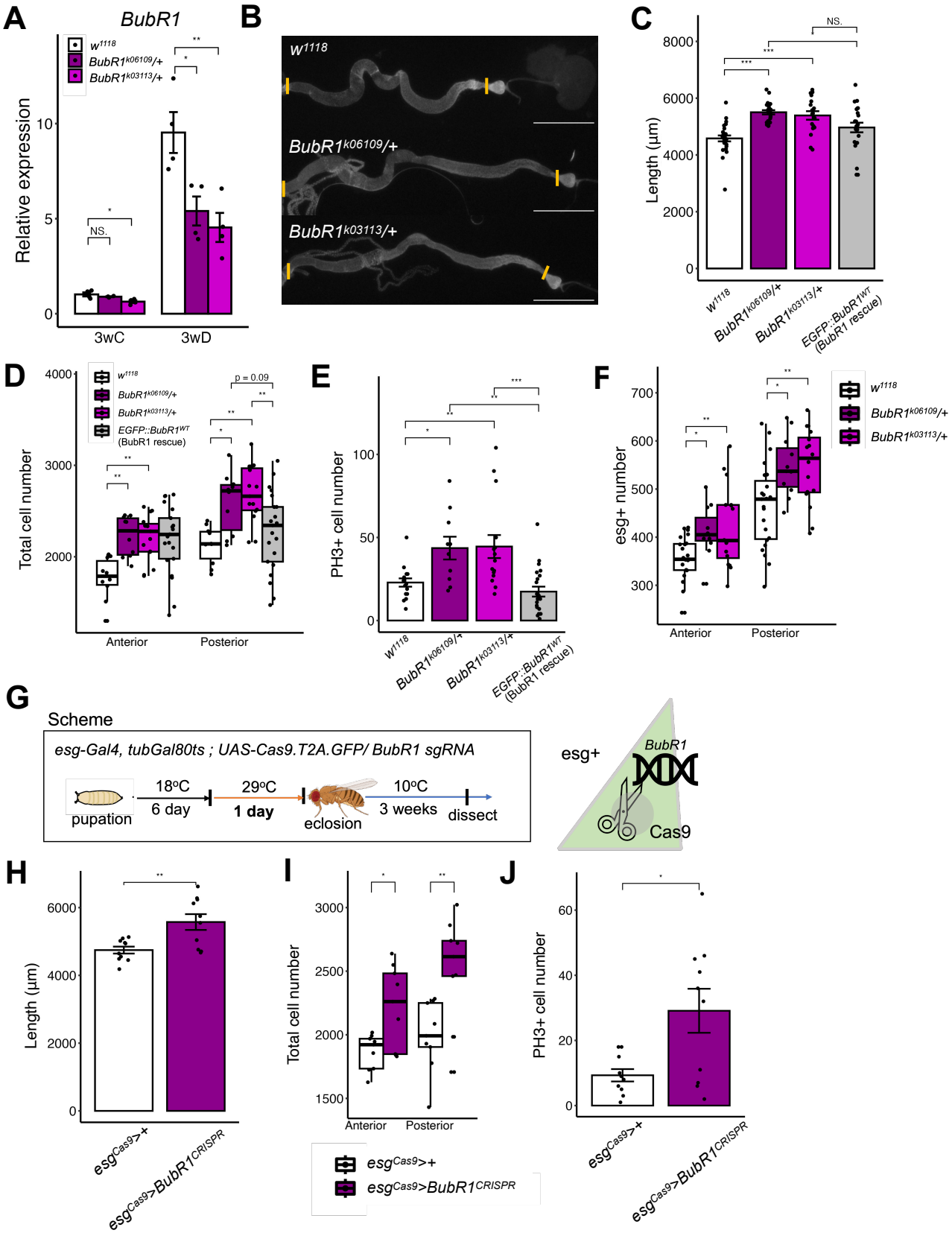
A
BubR1
w1118
BubR1k06109/+
BubR1k03113/+
Relative expression
NS.
3wC
3wD
B
w1118
BubR1k06109/+
BubR1k03113/+
C
Length (µm)
NS.
w1118
BubR1k06109/+
BubR1k03113/+
EGFP::BubR1WT (BubR1 rescue)
D
Total cell number
p = 0.09
EGFP::BubR1WT (BubR1 rescue)
Anterior
Posterior
E
PH3+ cell number
F
esg+ number
Anterior
Posterior
G
Scheme
esg-Gal4, tubGal80ts ; UAS-Cas9.T2A.GFP/ BubR1 sgRNA
pupation
18ºC
6 day
29ºC
1 day
eclosion
10ºC
3 weeks
dissect
esg+
BubR1
Cas9
H
Length (µm)
esgCas9>+
esgCas9>BubR1CRISPR
I
Total cell number
Anterior
Posterior
esgCas9>+
esgCas9>BubR1CRISPR
J
PH3+ cell number
esgCas9>+
esgCas9>BubR1CRISPR

Figure 5

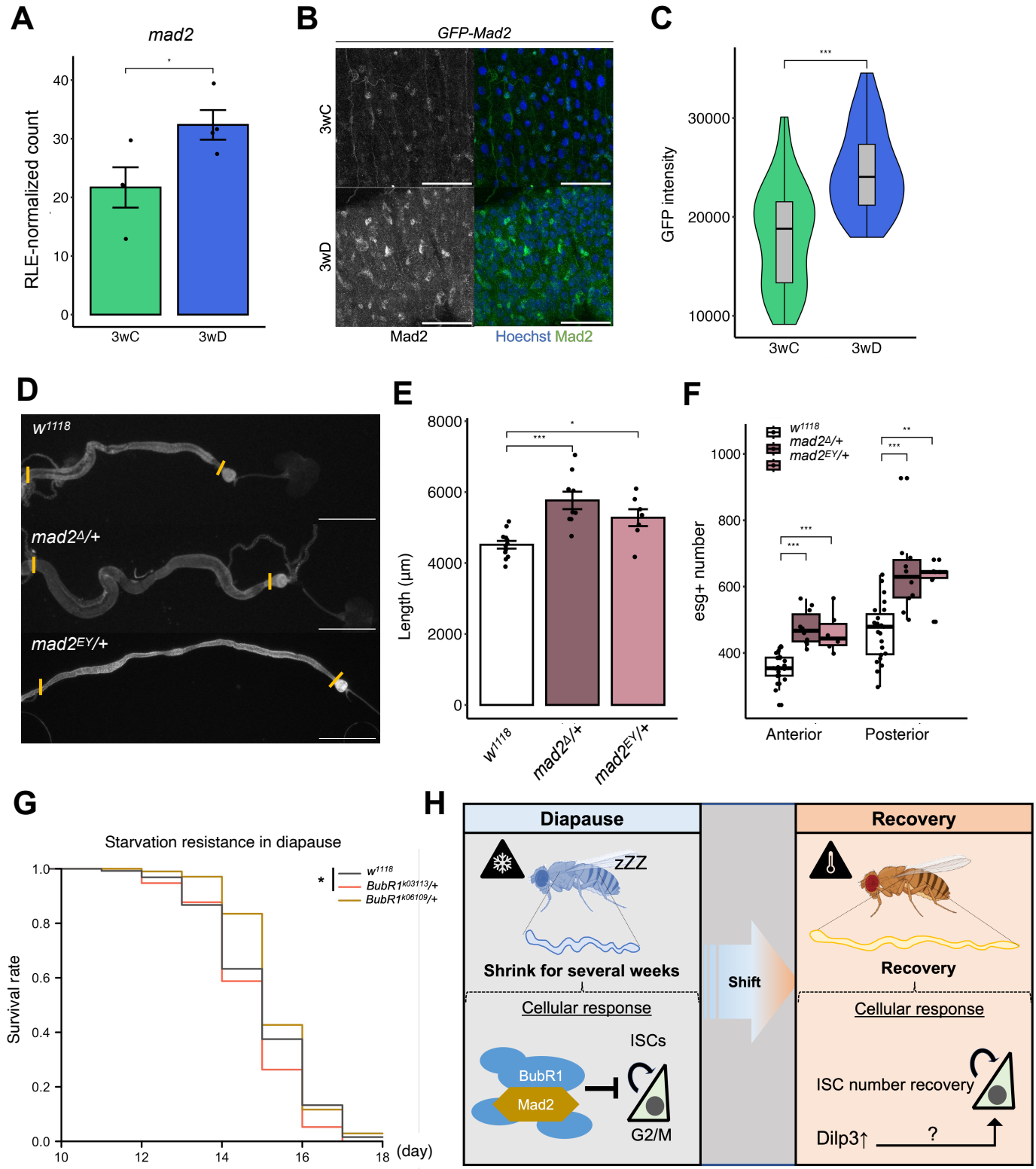
A
mad2
RLE-normalized count
3wC
3wD
B
GFP-Mad2
3wC
3wD
Mad2
Hoechst Mad2
C
GFP intensity
3wC
3wD
D
w1118
mad2Δ/+
mad2EY/+
E
Length (μm)
w1118
mad2Δ/+
mad2EY/+
F
esg+ number
w1118
mad2Δ/+
mad2EY/+
Anterior
Posterior
G
Starvation resistance in diapause
Survival rate
(day)
w1118
BubR1k03113/+
BubR1k06109/+
H
Diapause
Recovery
zZZ
Shrink for several weeks
Shift
Recovery
Cellular response
Cellular response
ISCs
BubR1
Mad2
G2/M
ISC number recovery
Dilp3↑
?